DTIC FILE COPY

AD-A223 696

DTIC ELECTE JUN 27 1990 S C D

REPORT DOCUMENTATION PAGE

1a. SECURITY CLASSIFICATION AU	1b. RESTRICTIVE MARKINGS
2b. DECLASSIFICATION/DOWNGRAD	3. DISTRIBUTION/AVAILABILITY OF REPORT: Unlimited
	DISTRIBUTION STATEMENT A Approved for public release Distribution Unlimited
4. PERFORMING ORGANIZATION R: CMTC-8945	5. MONITORING ORGANIZATION REPORT NUMBER(S): AFOSR-TR- 90-0570
6a. NAME OF PERFORMING ORGANIZATION: Penn State University	6b. OFFICE SYMBOL (If applicable):
6c. ADDRESS (City, State and ZIP Code): 227 Hammond Building, University Park, PA 16802	7a. NAME OF MONITORING ORGANIZATION: AFOSR
	7b. ADDRESS (City, State and ZIP Code): AFOSR/NA Bldg 410, Bolling AFB DC 20332-6448
8a. NAME OF FUNDING/SPONSORING ORGANIZATION: Air Force Office of Scientific Research	8b. OFFICE SYMBOL (If applicable): NA
	9. PROCUREMENT INSTRUMENT IDENTIFICATION NUMBER: Grant: AFOSR-87-0242
8c. ADDRESS (City, State and ZIP Code): Bolling Air Force Base, Washington, DC 20332-6448	10. SOURCE OF FUNDING NOS.

PROGRAM ELEMENT NO.	PROJECT NO.	TASK NO.	WORK UNIT NO.
61102F	2302	B2	

11. TITLE (Include Security Classification): Prediction and Control of Processing-Induced Residual Stresses in Composites Part II: AS4/PEEK Composite (Unclassified)

12. PERSONAL AUTHOR(S): Schulte, Kenneth J., Hahn, Hong T.

13a. TYPE OF REPORT	13b. TIME COVERED	14. DATE OF REPORT (Yr., Mo., Day)	15. PAGE COUNT
Final Report	FROM 6-87 TO 6-89	89-September-1	74

16. SUPPLEMENTARY NOTATION: See Part 1 - AD-A222 549

17. COSATI CODES			18. SUBJECT TERMS (Continue on reverse if necessary and identify by block number)
FIELD	GROUP	SUB. GR.	AS4/PEEK composites, Laminates, SFT, Thermoplastic Matrix Composites (JG)

19. ABSTRACT (Continue on reverse if necessary and identify by block number)

Residual stresses in symmetric cross-ply laminates were monitored by measuring the dimensionless curvature. The cooling rate was found to have a significant influence on the amount of residual stress in graphite/PEEK (APC-2) laminates. The transverse strain due to crystallization was not negligible and must be considered when predicting residual stresses for cooling rates of 75°C/min and lower.

The stress-free temperature for $[0_3/90_3]$ APC-2 laminates decreases with increasing cooling rate. Successive unconstrained heating/cooling provided the necessary environment for less stress relaxation allowing the specimens to move toward an equilibrium stress-free temperature (SFT) of 328°C. The SFT for any heating cycle was found to be equivalent to the previous cooling cycle SFT. The SFT is strongly dependent on geometrical constraint during thermal cycling because of the stress relaxation.

20. DISTRIBUTION/AVAILABILITY OF ABSTRACT	21. ABSTRACT SECURITY CLASSIFICATION
UNCLASSIFIED/UNLIMITED ☒ SAME AS RPT. ☑ DTIC USERS ☐	(U)

22a. NAME OF RESPONSIBLE INDIVIDUAL	22b. TELEPHONE NUMBER (Include Area Code)	22c. OFFICE SYMBOL
[redacted] George K. Haritos	(202) 767-0463	NA

DD FORM 1473, 83 APR — EDITION OF 1 JAN 73 IS OBSOLETE.

SECURITY CLASSIFICATION OF THIS PAGE (U)

Block 19 Continued...

A linear viscoelastic model was used to predict dimensionless curvatures. The model underestimates the residual stresses at high temperatures near the onset of crystallization and overestimates the stresses at temperatures below T_g. This was the result of not considering crystallization shrinkage or the presence of transverse cracking.

PENN STATE

CMTC - 8945

PREDICTION AND CONTROL OF PROCESSING-INDUCED RESIDUAL STRESSES IN COMPOSITES

PART II: AS4/PEEK COMPOSITE

K.J. SCHULTE
H.T. HAHN

OCTOBER 1989

Final Technical Report

Prepared for:
Air Force Office of Scientific Research
under AFOSR Grant 87-0242

Composites Manufacturing Technology Center
227 Hammond Building
The Pennsylvania State University
University Park, PA 16802

TABLE OF CONTENTS

CONTENTS (Continued)

LIST OF FIGURES

FIGURES (Continued)

FIGURES (Continued)

LIST OF TABLES

NOMENCLATURE

a	=	amorphous phase
A	=	area
c	=	crystalline phase
C	=	constant, geometric/material coefficient
d	=	diameter
D	=	creep compliance
e_L	=	longitudinal strain
e_T	=	transverse strain
E_L	=	longitudinal modulus
E_T	=	transverse modulus
f	=	fiber
G	=	shear modulus
h	=	height
H_c	=	enthalpy of crystallization
H_f	=	enthalpy of fusion
L	=	length
m	=	matrix
M	=	mass fraction
n	=	modulus ratio, E_T/E_L
N	=	number of observations
p	=	process
P	=	pressure
Q_c	=	cooling rate
R	=	radius of curvature
t, Δt_D	=	time, dwell time
T	=	temperature
T_{sf}	=	stress-free temperature
T_g	=	glass transition temperature
T_m	=	melt temperature
T_{oc}	=	onset of crystallization temperature
T_{ec}	=	end of crystallization temperature
TC	=	thermocouple
V	=	volume fraction

NOMENCLATURE (Continued)

W	=	weight fraction, width
X	=	longitudinal strength
Y	=	transverse strength
α_L	=	longitudinal thermal expansion coefficient
α_T	=	transverse thermal expansion coefficient
ρ	=	density
ν	=	Poisson's ratio
τ	=	time
ζ	=	reduction time

ABSTRACT

Residual stresses in symmetric cross-ply laminates were monitored by measuring the dimensionless curvature. The cooling rate was found to have a significant influence on the amount of residual stress in graphite/PEEK (APC-2) laminates. The transverse strain due to crystallization was not negligible and must be considered when predicting residual stresses for cooling rates of 75°C/min and lower.

The stress-free temperature for $[0_3/90_3]$ APC-2 laminates decreases with increasing cooling rate. Successive unconstrained heating/cooling provided the necessary environment for less stress relaxation allowing the specimens to move toward an equilibrium stress-free temperature (SFT) of 328°C. The SFT for any heating cycle was found to be equivalent to the previous cooling cycle SFT. The SFT is strongly dependent on geometrical constraint during thermal cycling because of the stress relaxation.

A linear viscoelastic model was used to predict dimensionless curvatures. The model underestimates the residual stresses at high temperatures near the onset of crystallization and overestimates the stresses at temperatures below T_g. This was the result of not considering crystallization shrinkage or the presence of transverse cracking.

ACKNOWLEDGEMENTS

The authors would like to acknowledge Lt. Col. George K. Haritos, Air Force Office of Scientific Research, as contract monitor for this project. McDonnell Aircraft Company is acknowledged for supplying the APC-2 (Gr/PEEK) prepreg material. We are also very grateful to Jesus Pascual for his efforts in converting the many figures in this report from MS-DOS® to a Macintosh® format. A very special thank-you is given to Teresa Jones for her assistance with the typing.

1. INTRODUCTION

Thermoplastic matrix composites are now being considered for many commercial, space, and aircraft applications. The use of these materials requires knowledge of their properties and how they change with environmental conditions, processing techniques, and load histories.

Thermoplastics can be of two forms: amorphous and crystalline. The crystalline polymers are semi-crystalline because they can not be truly 100% crystalline. Table 1 lists several common crystalline and amorphous thermoplastics. The primary advantages of using thermoplastic matrix composites over thermoset matrix composites are reprocessibility, short process cycle, higher impact strength, higher fracture resistance, and long shelf life. Other advantages and disadvantages for crystalline and amorphous thermoplastics are listed in Table 2.

Thermoplastic matrix composites typically require a high processing temperature (350°-400°C) to melt and consolidate. It is the thermal shrinkage mismatch between the fiber and matrix during cooling down from these high temperatures that introduces the majority of the residual stresses in the composite. For semi-crystalline thermoplastic matrix composites, the additional source of residual stresses is the shrinkage resulting from crystallization. Of course, some of these residual stresses will be relaxed in time. However, the resultant residual stresses may be high enough to cause ply cracking before any load is ever applied, degrade impact resistance, and deteriorate dimensional stability.

Both the crystallization shrinkage and stress relaxation depend on the process cycle. For example, a fast cool-down usually results in lower crystallinity and hence is expected to give lower residual stresses. However, a fast cool-down will also result in less stress relaxation negating the aforementioned beneficial effect. Furthermore, residual stresses can be reduced by annealing through stress relaxation. Therefore, it is necessary to develop a process cycle and an annealing procedure to reduce residual stresses.

1.1 Objective

The objectives of the present research are four fold. First, determine the relationship between residual stress and processing variables such as temperature, pressure, and time for a semi-crystalline thermoplastic matrix composite (AS4 graphite fiber/polyetheretherketone (PEEK) matrix). Second, measure the crystallinity resulting from various process cycles and determine its

Table 1. Crystalline and Amorphous Thermoplastics.

Crystalline	Amorphous
Polypropylene	Polystyrene
Nylon	Acrylic
Acetal	Polycarbonate
Polyphenylene sulfide (PPS)	Polysulfone (PSF)
Polyetheretherketone (PEEK)	Polyether sulfone (PES)
Polyethylene terephthalate (PET)	Polyetherimide (PEI)
Polyarylamide (J polymer)	Polyamide-imide (PAI)

Table 2. Advantages and Disadvantages of Thermoplastic Matrix Composites.

ADVANTAGES

- **Crystalline Polymers**
  - Resistance to Organic Solvents
  - Resistance to Dynamic Fatigue
  - Temperature Range Increased by Glass, Carbon, or Graphite Reinforcement
  - Retention of Ductility on Short Term Heat Aging

- **Amorphous Polymers**
  - Transparent
  - Low and Uniform Mold Shrinkage
  - Low and Uniform Coefficient of Thermal Expansion
  - Minimal Post Mold Shrinkage
  - Properties are Less Temperature Dependant

- **General**
  - Reprocessibility
  - Long Shelf Life
  - Short Process Cycle
  - Thermo-forming
  - Higher Impact strength and Fracture Resistance Compared to Thermosets
  - Ease of Handling (no tackiness)

DISADVANTAGES

- High Material Costs
- Viscoelastic Behavior
- High Process Temperature

contribution to residual stresses. Third, develop a predictive methodology for residual stresses. Last, recommend an optimum process cycle including annealing to control residual stresses.

2. LITERATURE REVIEW

The material chosen for this study was a continuous graphite fiber (AS4) preimpregnated with polyetheretherketone (PEEK), a semi-crystalline thermoplastic resin. This prepreg tape is commercially available from Imperial Chemical Industries (ICI), Inc. under the generic title of Aromatic Polymer Composite (APC) [1]. Specifically, the APC-2 formula, available since 1982, has been used in this study in an effort to draw upon the large amount of data available in the literature.

2.1 Mechanical Properties

Numerous papers have been written on both neat PEEK and APC-2 composites. Because of the crystalline nature of PEEK and its interaction with the graphite fibers during crystallization, it is more important to show the composite properties than the constituent properties when making macroscopic inferences. Tables 3, 4, and 5 list fiber, matrix, and composite properties, respectively, as found in the literature. The single most comprehensive source for APC-2 properties was Reference [2]. Tsai [3] lists typical ply data for AS4/PEEK as well as other popular composite systems, but does not cite any references or how they were acquired. For a more in depth study of specific APC-2 properties, the following references should be consulted:

Property	References
Tensile and Flexural Strength	2,4,5
Compressive Strength	6-9
Impact Strength	8-12
Fracture Toughness	13-15
Fatigue Strength	16,17
Matrix Fractography	6,18,19

Table 3. Hercules AS4 Magnamite® Graphite Fiber Properties [20-22].

Tensile Strength (a), σ_T		3795 MPa
Tensile Modulus (a), E_T		235 GPa
Ultimate Elongation (a), e_U		1.53%
Density, ρ		1.80 g/cm^3
Specific Heat	@ 75°C	0.22 cal/g°C
	@ 175°C	0.27 cal/g°C
Fiber Diameter, d_f		7 μm
Poisson's Ratio, υ		0.28
Longitudinal Thermal Expansion, α_L		-0.3 μ/°C
Transverse Thermal Expansion, α_T		18 μ/°C
Thermal Conductivity, k		1.02(10^{-3}) cal/(sec cm^2(°C/cm))
Thermal Diffusivity		5.701(10^{-3}) cm^2/sec
Electrical Resistance (12K tow)		0.32 Ω/cm
Electrical Resistivity		1.53(10^{-3}) Ω cm

(a) Calculated from composite laminate test data [22].

Table 4. ICI Victrex® Polyetheretherketone (PEEK) Properties(a) [7,20,21,23-25].

Tensile Strength, σ_T		100 MPa
Yield Strength, σ_y		96.9 MPa
Impact Strength		85 J/m
Tensile Modulus, E_T		3.45 GPa
Shear Modulus, G		1.22 GPa
Flexural Modulus, E_F		3.79 GPa
Ultimate Elongation, e_U		> 100%
Density:	amorphous, ρ_a	1.2626 g/cm^3
	crystalline, ρ_c	1.4006 g/cm^3
Specific Heat		0.32 cal/g°C
Poisson's Ratio, υ		0.378
Heat of Fusion (crystalline)		130 J/g
Thermal Conductivity, k		0.6(10^{-3}) cal/(sec cm^2(°C/cm))
Thermal Diffusivity		1.485(10^{-3}) cm^2/sec
Heat Distortion Temperature, T_{HD}		159°C @ 1.82 KPa
Glass Transition Temperature, T_g		155°C
Melt Temperature, T_m		335°C
Crystalline Temperature Range		
	Onset Temperature, T_{oc}	~320°C
	End Temperature, T_{ec}	~180°C

(a) Grade 450G neat PEEK

Table 5. APC-2 (Gr/PEEK) Properties [2-4,20,26,27].

Longitudinal Modulus, E_L	135.2 ± 8.5 GPa
Transverse Modulus, E_T	9.2 ± 0.4 GPa
Longitudinal Flexural Modulus, E_{LF}	130.0 ± 1.7 GPa
Transverse Flexural Modulus, E_{TF}	10.3 ± 0.3 GPa
Shear Modulus, G	4.90 GPa
Longitudinal Tensile Strength, X	2090 ± 80 MPa
Transverse Tensile Strength, Y	80 ± 1.6 MPa
Longitudinal Compressive Strength, X'	1094 ± 46 MPa
Transverse Compressive Strength, Y'	200 MPa
Longitudinal Flexural Strength, X_F	1872 ± 49 MPa
Transverse Flexural Strength, Y_F	140 ± 0.4 MPa
Longitudinal Tensile Strain, e_L	1.45 ± 0.2%
Transverse Tensile Strain, e_T	1.00 ± 0.2%
Longitudinal Compressive Strain, e'_L	0.82%
Transverse Compressive Strain, e'_T	2.35%
Density, ρ	1.480 g/cm^3
Poisson's Ratio, υ_{LT}	0.35
Fiber Volume Fraction, V_f	0.62
Ply Thickness, h_o	0.125 mm
Longitudinal Thermal Expansion, α_L	0.5 μ/°C < Tg
	1.0 μ/°C > Tg
Transverse Thermal Expansion, α_T	30 μ/°C < Tg
	75 μ/°C > Tg
Thermal Conductivity, k	0.76(10^{-3}) cal/(sec cm^2(°C/cm))
Thermal Diffusivity	1.656(10^{-3}) cm^2/sec
Glass Transition Temperature, T_g	143°C
Stress-Free Temperature, T_{sf}	328°C (fully crystalline)
Melt Temperature, T_m	343°C

2.2 Viscoelastic Behavior

PEEK, like all polymers, exhibits viscoelastic properties when loaded under high temperature conditions. At temperatures above the glass transition, T_g, PEEK will begin to show a significant deterioration in properties [28,29]. Extensive work on the complex modulus [30] has shown that the temperature, magnitude and width of the peak loss modulus in the glass transition region are sensitive to the cooling rate. The cooling rate also strongly affects the storage modulus in the rubbery region, but has little effect in the glass region. The tensile creep compliance was shown to decrease with increasing crystallinity (T_{test} = 130°C) for 45G grade neat PEEK [31] . Ogale and McCullough [31] have estimated the crystalline modulus to be 30 GPa using the Aggregate Model.

Hashin et al. [32] have developed a method of analysis for determining the thermoviscoelastic properties of unidirectional composites consisting of transversely isotropic elastic fibers and any linear viscoelastic matrix. Analytical results for a carbon fiber/3502 epoxy system show significant effects of matrix thermoviscoelasticity. The creep strain was found to increase as well as a softening of the initial and time-dependent portions of the composite response as temperature was increased. The magnitude of accumulated viscoelastic strain was seen to be small for reversed loading and represented a phase lag between temperature change and strain response. No experimental data was offered for comparison.

Viscoelastic effects have been included in residual stress prediction for graphite/epoxy composites [33-35] and a thermoplastic matrix composite [36]. Chapman et al. [36] have developed a finite difference FORTRAN computer model to predict in-plane residual stresses accounting for surface cooling history, ply orientation, constituent elastic properties, heat transfer parameters, and viscoelastic and thermal contraction behavior of APC-2 composites. The degree of crystallinity in APC-2 was reported to be an insignificant factor in mechanical properties. This is contrary to previous work performed at Penn State [5] and elsewhere [37-39] which showed that modulus and strength properties varied with the degree of matrix crystallinity. Although the model by Chapman appears to be comprehensive, additional experimental results are needed to verify the model.

2.3 Cooling Rates and Crystallinity

Fusion of APC-2 prepreg has been reported to occur in a matter of seconds at 380°C [26,40]. Hence, the most important process variable is the temperature and the rate of cooling. Numerous studies [5,23,24,26,36,38,39,41-49] have shown that increasing the cooling rate decreases the amount of crystallinity found in the APC-2 matrix. Crystallization takes place in the approximate temperature range of 180° to 320°C with the maximum crystallization rate occurring around 275°C. Thus, the rate of crystallization and final crystallinity of the matrix is determined by the rate at which the material passes through the crystallization range. The effects of crystallinity on APC-2 mechanical properties are found in [5,37-39]. In general, the crystalline phase acts as a reinforcement in the matrix, thereby giving higher strength and modulus, but lower fracture toughness. Fibers in the matrix serve as nucleation sites [50,51] and is likely to alter the crystallization kinetics such that the measured crystallinities are higher in APC-2 than in neat PEEK.

2.4 Residual Stresses

Residual stresses in composite laminates have been determined by various methods such as the curvature of unbalanced cross-ply laminates [33,52-56], embedded strain gages [57], first ply failure [58], milling [56], and a technique called a process simulated laminate [36,59]. The latter technique uses superposition of residual stresses in several thin laminates processed together (separated by release plies) to predict the residual stress in a laminate of equivalent thickness. Residual stresses develop during crystallization for semi-crystalline thermoplastics and below the glass transition temperature for amorphous thermoplastics [55]. Residual stresses at room temperature were found to be large enough to cause ply cracking in amorphous thermoplastics [25,60]. Nairn and Zoller [25] reported no evidence of ply cracking in APC-1 (the precursor of APC-2) laminates whereas a small amount of ply cracking was seen by Jeronimidis and Parkyn [56].

2.5 Stress-Free Temperature

The stress-free temperature T_{sf} is the temperature at which residual stresses disappear. Previous work [56] with varying laminate thicknesses has found the T_{sf} to be 310°C for APC-2 with a cooling rate of 3°C/min. The T_{sf} for APC-1 was found by similar methods [25] to be 328°C on heating and 319°C on cooling.

3. EXPERIMENTAL PROCEDURE

The main objective of the experimental phase of the present research was to determine how residual stresses were affected by the cooling rate, applied fabrication pressure, and post-fabrication thermal cycling. Warpage of asymmetric cross-ply laminates was used as an indirect measure of residual stresses.

3.1 Processing Method

A multiple specimen mold shown in Figure 1 was used to fabricate two 50.8 mm x 152.4 mm and two 25.4 mm x 152.4 mm specimens in a single process cycle. The matched die mold was fabricated from precision ground high carbon steel and cured using Mono-Coat® E63 as recommended by the manufacturer, Chem-Trend Inc. Although reapplication of the Mono-Coat release agent was found to be unnecessary, a light coating was applied before each process run along with a Kapton release film to consistently achieve a high quality surface finish.

Laminate configurations included $[0_6]$, $[90_6]$ and $[0_3/90_3]$. The unidirectional laminates were fabricated as 50.8 mm x 152.4 mm and later cut to the standard 25.4 mm x 152.4 mm configuration for testing.

A 12-ton microprocessor controlled Tetrahedron Materials Test Press (MTP-14), shown in Figure 2, was used to compression mold the APC-2. A typical process cycle was to heat up at 14°C/min to a process temperature T_p, dwell for a given duration Δt_D, then cool at the desired rate Q_c to room temperature. The applied pressure P_p was constant throughout the entire temperature history. The chosen processing parameters are:

T_p Temperature (°C)	Δt_D Dwell Time (min)	P_p Pressure (MPa)	Q_c Cooling Rate (°C/min)
380	15	0.34	< 1
400	30	0.69	50-75
		1.34	> 650

For slow cooling rates, <1°C/min, the MTP was used for both heating and cooling cycles. For medium cooling rates, 50°-75°C/min, the mold was transferred to a Tinius Olsen Testing Machine

after the dwell cycle and placed between two aluminum cooling plates. Room-temperature water pumped through the plates at 10 gpm gave the medium cooling rates consistently.
Figure 3 illustrates the 50°-75°C/min cooling rate set-up. High cooling rates (i.e. >650°C/min) were achieved using an ice/water quench on the testing machine, which was used to maintain a processing pressure. An Omega 900 series data acquisition system was used in conjunction with an AT-compatible microcomputer to record the temperature history from type J thermocouples during processing.

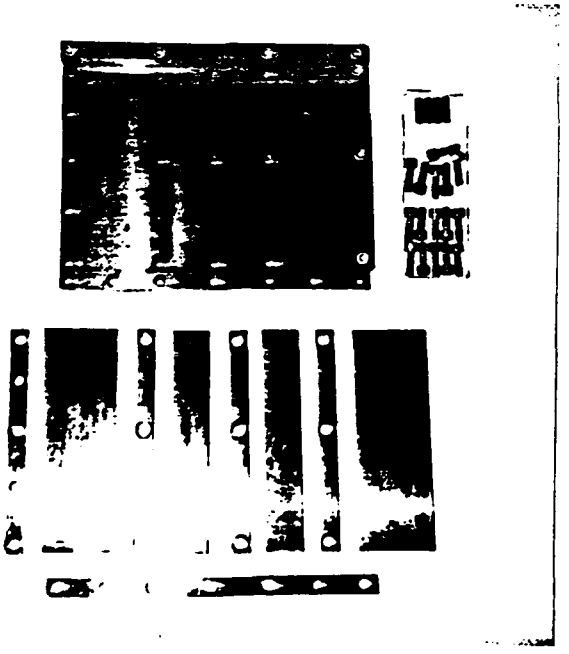

Figure 1. Match Die Mold for Fabricating Multiple Specimens.

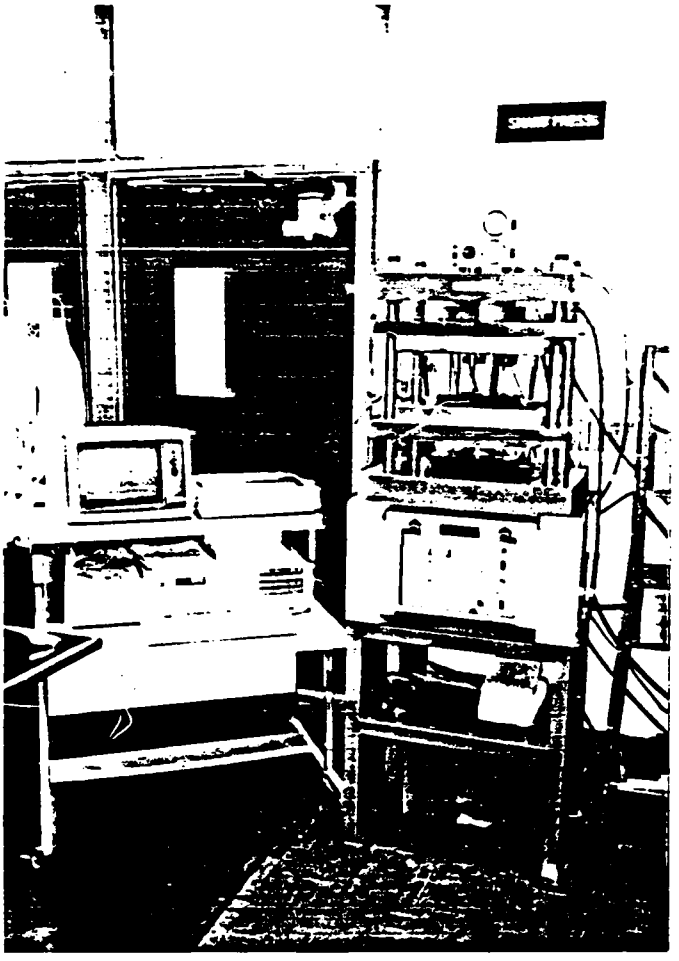

Figure 2. Compression Mold Press and Data Acquisition System Used in Processing APC-2 Specimens.

(a)

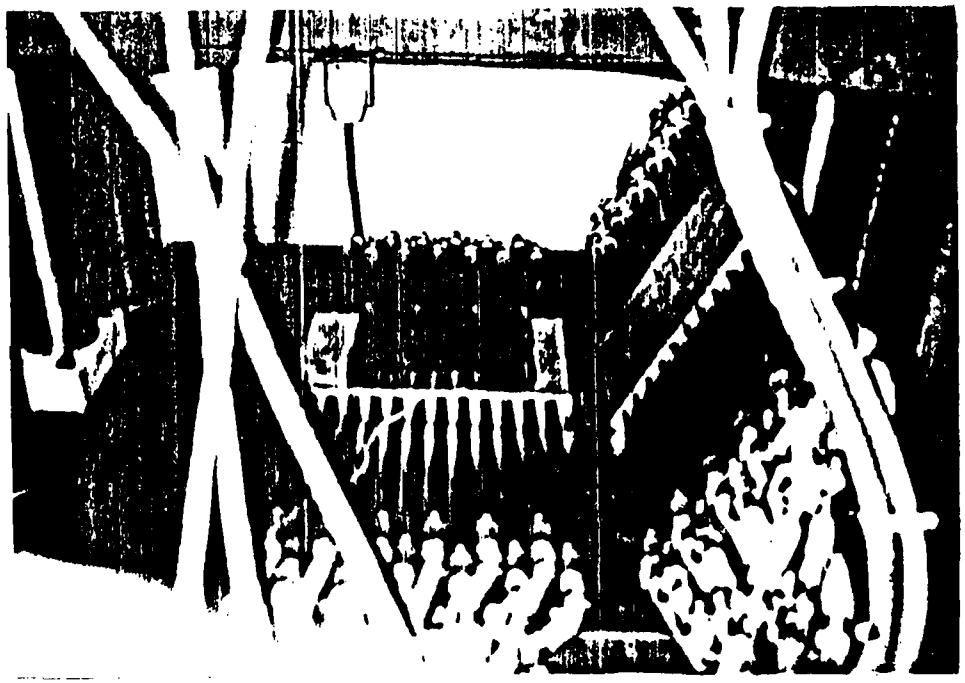

(b)

Figure 3. Set-Up for Achieving 50°-75°C/min Cooling Rates With the Multiple Specimen Mold.

3.2 Dimensionless Curvature

The radius of curvature of the 25.4 mm x 152.4 mm [$0_3/90_3$] specimen in the 0° direction was measured by placing the specimen on a reference block and measuring the height deviation at several locations. Figures 4 and 5 illustrate the method. A reference block 51 mm wide was used to reduce the unintentional flex and to allow readings near the specimen ends. Height and thickness measurements were recorded for distances of 38.1 mm, 76.2, and 114.3 mm from the specimen end. The radius was calculated from [61]

$$R = \frac{\left(\frac{c}{2}\right)^2 + (h - t)^2}{2(h - t)} \tag{1}$$

where: c = reference block width
h = measured height
t = specimen thickness.

Since the radius of curvature is dependent on the laminate thickness [56], the curvature was normalized by dividing the thickness by the radius of curvature. Any change observed in the dimensionless curvature, t/R, along the specimen length would be an indicator of possible non-uniform cooling, crystallization, or the presence of microcracks.

3.3 Stress-Free Temperature

The purpose of the stress-free temperature (SFT) study was to determine the temperature at which residual stresses begin to build up and record the temperature dependence of the dimensionless curvature.

The [$0_3/90_3$] 25.4 mm x 152.4 mm specimens were temperature cycled in an Applied Test Systems, Inc. temperature chamber capable of 400°C maximum temperature. Figure 6 shows the [$0_3/90_3$] specimen mounted on a 127 mm reference block inside the chamber with a 0.4 mm metal scale for reference. Seven type J thermocouples (TC) were used with an Omega 900 data acquisition system to record the chamber and specimen temperatures. A Panasonic WV-3240/12X video camcorder was used to visually measure the specimen deflection and to provide a permanent record of the events. A Reichert-Jung optical fiber lamp was used to provide lighting to the specimen and reference scale. Figures 7(a) and (b) illustrate the set-up used in the SFT study.

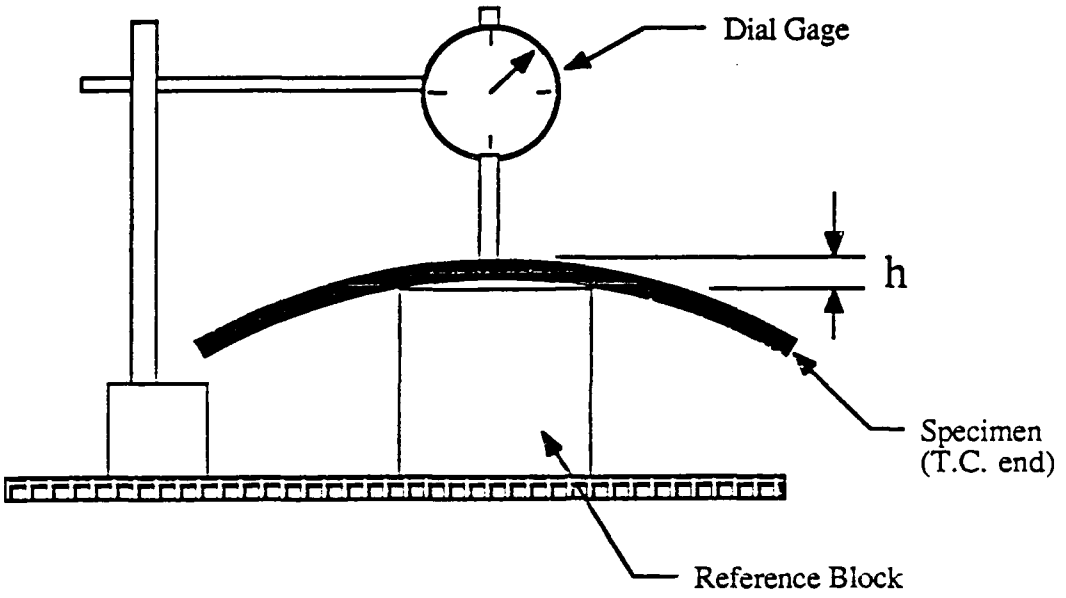

Figure 4. Measurement of Local Height Deviation for Curvature Specimens.

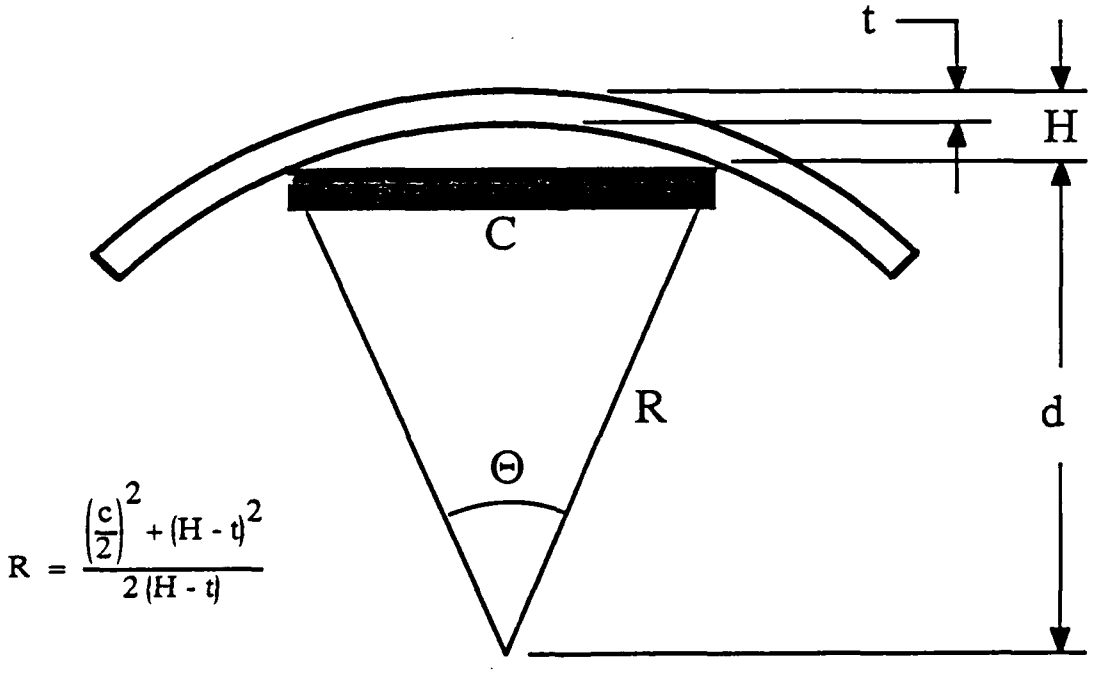

Figure 5. Geometry Used to Calculate the Radius of Curvature.

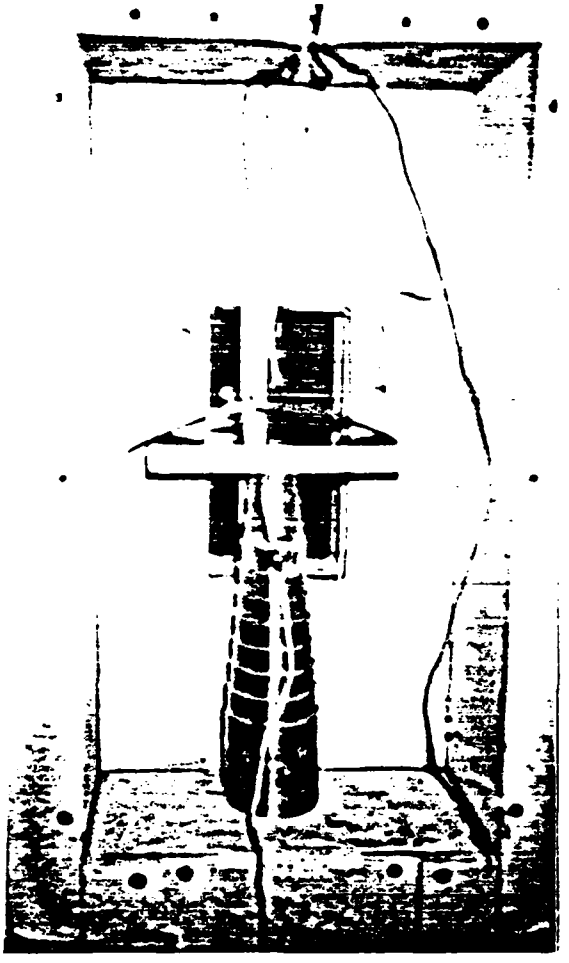

Figure 6. Temperature Chamber Set-Up During Stress-Free Temperature Study.

(a)

Overall set-up.

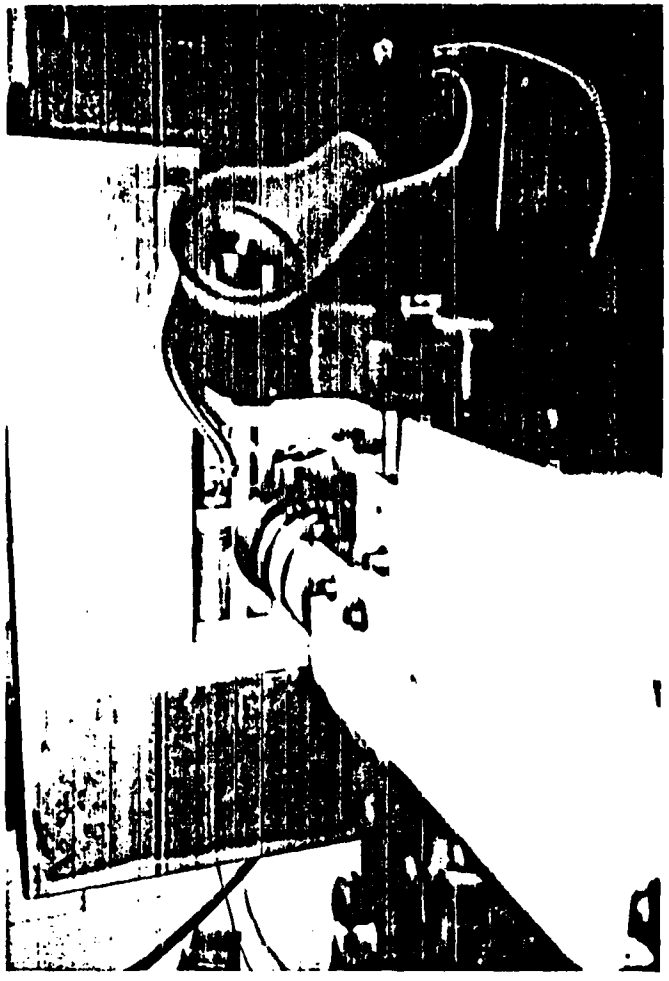

(b)

Close-up view of temperature chamber window.

Figure 7. Video Camera and Data Acquisition System Set-Up for SFT Study.

The SFT study was performed in two stages. In Phase I, the cooling rate was not controlled while in Phase II the cooling rate was controlled to 1° ± 0.5°C/min by a LFE model 2010 controller. The heating rate was controlled to 3°± 0.5°C/min for both test series.

3.4 Differential Scanning Calorimetry

A Perkin Elmer 7500 thermal analysis system with a DSC7 module was used to measure the enthalpy of crystallization as a function of temperature for as processed APC-2 specimens.

The mass fraction crystallinity, M_c, is defined by [45]

$$M_c = \frac{H_c}{(1 - M_f) H_f} \tag{2}$$

where H_c is the enthalpy of crystallization per unit mass of the composite, H_f is the enthalpy of fusion per unit mass of the crystalline phase, and M_f is the fiber weight fraction. Equation (2) can be rewritten in terms of the crystalline and amorphous matrix densities by,

$$M_c = \frac{\left(\frac{\rho_f}{\rho_a} - 1\right) V_f + 1}{\left[\frac{\rho_f(\rho_c - \rho_a)}{\rho_a \rho_c}\right] V_f + (1 - V_f)\frac{H_f}{H_c}} \tag{3}$$

where:

ρ_f = fiber density (1.80 g/cm³) [22]

ρ_a = amorphous matrix density (1.263 g/cm³) [45]

ρ_c = crystalline matrix density (1.400 g/cm³) [45]

H_f = enthalpy of fusion (130 J/g) [48]

H_c = enthalpy of crystallization (J/g)

V_f = fiber volume fraction (0.62 by experiment)

The crystallinity of several high Q_c specimens was measured at several locations and related to the curvature at the same point. Figure 8 illustrates the locations where the DSC specimens were obtained. DSC specimens taken from the TC end of the specimen were used to have a better correlation to the cooling rate.

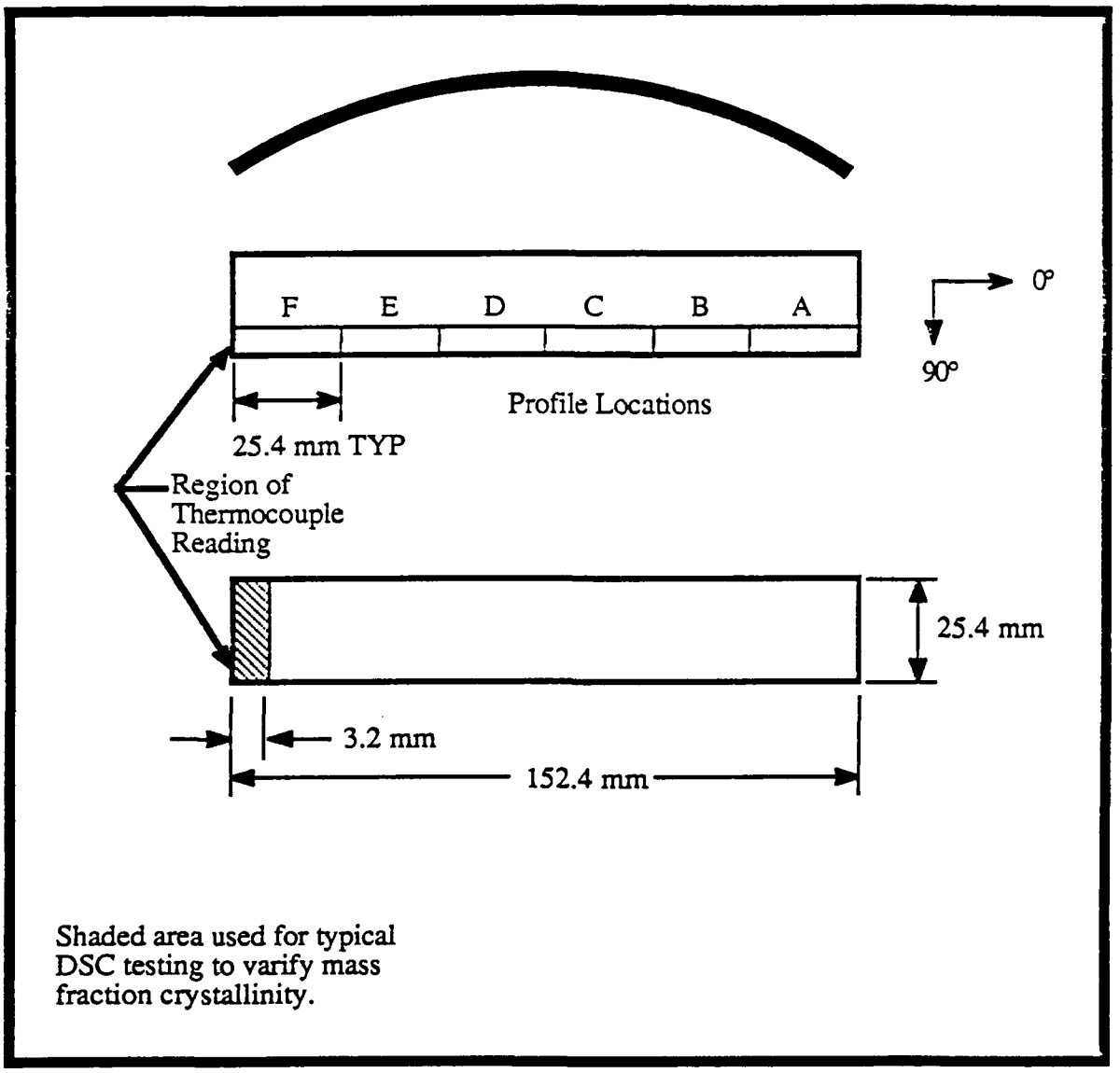

Figure 8. DSC Profile Study of Curvature Specimen and Typical DSC Specimen Source.

3.5 Fiber Volume Fraction

There are two techniques commonly employed to determine the volume fraction of fibers in a composite: chemical matrix digestion and photomicrography [62]. The latter technique was used in the present research. The fiber volume fraction is determined as

$$V_f = \frac{A_f}{A} \tag{4}$$

where A is the area of a selected region of the photomicrograph and A_f is the total fiber area in the selected region. Photomicrographs were taken using a Unitron® metallographic microscope and a Lasertec® scanning laser microscope.

3.6 X-Ray Radiography

X-ray radiography was used to determine the presence and number of cracks in the as-processed APC-2 specimens. Specimens, 0.76 mm x 7.6 mm x 50.8 mm, were cut from a 25.4 mm x 152.4 mm $[0_3/90_3]$ specimens, Figure 9, using a water cooled Felter® table saw with a diamond blade. In addition, full size $[0_3/90_3]$ specimens (as processed and SFT cycled) were used for comparison.

The specimen strips were immersed in a 1,4-Diiodobutane solution for 24 hours to allow full penetration of the dye into the composite. The full-scale curvature specimens were forced flat (i.e. initial post-processing state) and immersed in the 1,4-Diiodobutane solution for 2 hours. All specimens were then X-rayed using a Faxitron® radiographic inspection unit.

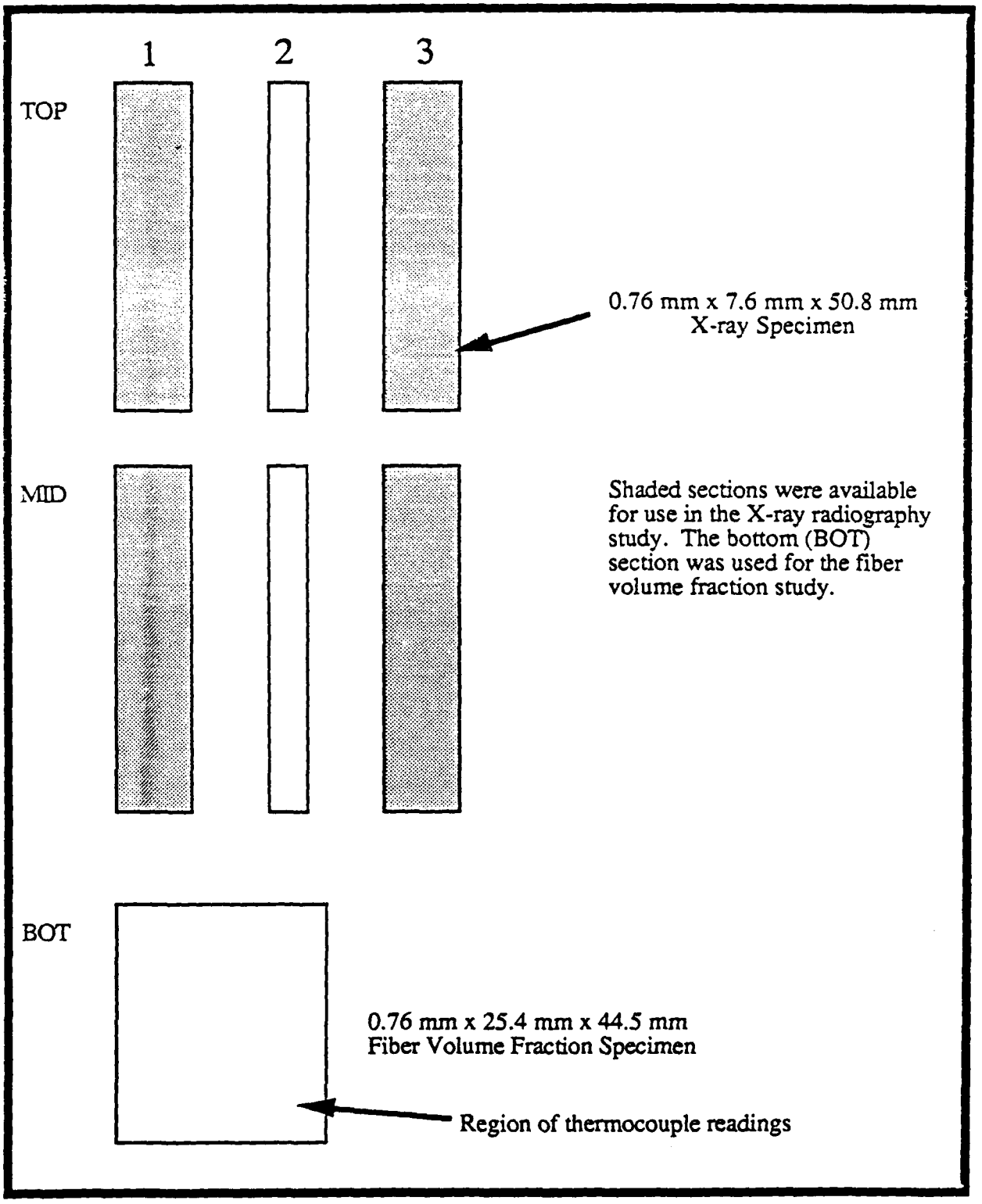

Figure 9. Cut-Up of Curvature Specimens for X-Ray Radiography Study.

4. ANALYSIS

The build-up of residual stresses in semi-crystalline thermoplastic matrix composites is dependent on thermal and chemical changes in the matrix. Thermal residual stresses develop due to the mismatch in thermal expansion coefficients of the fiber and the matrix. Crystallization results in shrinkage giving rise to additional stresses during cooling. The dimensionless curvature, t/R, of asymmetric cross-ply laminates is the result of these residual stresses.

4.1 Elastic Analysis

The early analyses of residual stresses in composites were based on the assumption of elastic behavior [63,64]. These analyses were for thermoset matrix composites after complete cure and, hence, did not account for chemical shrinkage. Several analyses [44,55,56] used the Timoshenko [65] bimetallic strip theory (BST) with temperature-dependent properties for thermoplastic composites. However, these analyses did not take into account shrinkage due to crystallization and was found to under predict the initial residual stress buildup and over predict the stresses at temperatures below the glass transition temperature.

For long and narrow strips of a $[0_3/90_3]$ laminate used in the present study, the dimensionless curvature is given by

$$\frac{t}{R} = C(e_L - e_T) \tag{5}$$

where t is the laminate thickness, R is the radius of curvature, and e_L and e_T are the longitudinal and transverse expansional strains, respectively. The factor C is related to the elastic moduli by [52]

$$C = \frac{24\left[1 + \left(1 - 2\upsilon - \upsilon^2\right)n + \left(2\upsilon^3 - \upsilon^2\right)n^2\right]n}{\left[1 + 15\,n + \left(15 - 16\,\upsilon^2\right)n^2 + \left(1 - 16\,\upsilon^2\right)n^3\right]} \tag{6}$$

where υ is the major Poisson's ratio and n is the modulus ratio E_T/E_L. Note that all properties are measured at the temperature of interest.

The expansional strain e consists of two parts: thermal strain e^T and crystallization strain e^c.

$$e_L = e_L^T + e_L^c \tag{7}$$

$$e_T = e_T^T + e_T^c \tag{8}$$

The expansion strains are measured from a stress-free temperature, T_{sf}. The SFT ranges from the melt temperature, T_m, to the onset of crystallization temperature, T_{oc}.

The thermal strains can be written in terms of the temperature-dependent thermal expansion coefficients:

$$e_L^T = \int_{T_{sf}}^{T} \alpha_L(T)\, dT \tag{9}$$

$$e_T^T = \int_{T_{sf}}^{T} \alpha_T(T)\, dT \tag{10}$$

The longitudinal expansional strain e_L is dominated by the fibers and hence,

$$e_L^c = 0 \tag{11}$$

The transverse crystallization strain can be obtained from the matrix crystallization strain $e^c{}_m$ using the micromechanics equation in [3]

$$e_T^c = (1 + \upsilon_m)\, V_m\, e_m^c \tag{12}$$

where υ_m and V_m are the Poisson's ratio and volume fraction, respectively, of the matrix.

During processing, the PEEK resin changes from a fully amorphous at the melt state to a semi-crystalline with a mass fraction crystallinity, M_c. The resulting volume change is given by

$$\frac{\Delta V_m}{V_m} = M_c\left[1 - \frac{\rho_a}{\rho_c}\right] \tag{13}$$

where ρ_a and ρ_c are the densities of the amorphous and crystalline phases, respectively. Since

$$e_m^c = \frac{1}{3}\frac{\Delta V_m}{V_m}$$

the transverse crystalline strain is therefore

$$e_T^c = \frac{1}{3}\left(1+\upsilon_m\right) V_m M_c\left(1-\frac{\rho_a}{\rho_c}\right) \tag{14}$$

Substituting Eq. (3) into (14) gives the final equation for the transverse shrinkage strain

$$e_T^c = \frac{1}{3}\left(1+\upsilon_m\right)\left(1-\frac{\rho_a}{\rho_c}\right)\left[\frac{\left(\frac{\rho_f}{\rho_a}-1\right)V_f + 1}{\left[\frac{\rho_f\left(\rho_c-\rho_a\right)}{\rho_a\rho_c}\right]\frac{V_f}{\left(1-V_f\right)} + \frac{H_f}{H_c}}\right] \tag{15}$$

4.2 Viscoelastic Analysis

The viscoelastic properties of neat PEEK have been previously investigated [30-32] and found to be significant above 155°C which is the glass transition temperature for neat PEEK. Several models have been developed for epoxy and thermoplastic matrices [33,34,36,44]. The analysis taken from [33] are described in Part I of the Final Report [66] for IM6/BMI materials.

The model assumes linear thermorheologically simple viscoelastic behavior and accounts for both volume shrinkage due to crystallization and specimen geometry. The time-dependent dimensionless curvature is given as

$$\frac{t}{R}(t) = \int_0^t C(t)\left[\xi(t) - \xi(\tau)\right]\frac{d}{d\tau}\left(e_L(\tau) - e_T(\tau)\right)d\tau \tag{16}$$

where C, e_L, and e_T are given by Eqs. (6), (7) and (8), respectively. $\xi(t)$ and $\xi(\tau)$ are reduced times found by integrating the shift factor associated with the matrix transient thermal response [66].

5. RESULTS AND DISCUSSION

5.1 Effect of Cooling Rate on Curvature Development

As described in Section 3.1, asymmetric cross-ply laminate specimens, $[0_3/90_3]$, were fabricated and the resulting curvatures were measured as an indicator of the amount of residual stress. Table 6 lists the dimensionless curvatures found at various cooling rates. The specimen identification code is explained in Figure 10.

By making use of a 51 mm reference block in calculating the radius of curvature (Figure 5), it was possible to obtain 3 independent readings along the specimen. The dimensionless curvature was found to be relatively uniform at each of the cooling rates (within 5% of the mean). The largest variations in t/R were found in specimens processed at the lowest pressure (0.34 MPa) and at the highest process temperature (400°C). The reason is that variability in the cooling rate across the surface of the specimen will result in a different degree of crystallization and stress relaxation from point to point. The time-temperature relation for cooling from a processing temperature of 380°C was found to be non-linear for cooling rates greater than 50°C/min. The data of Table 6 shows the curvature is decreasing with increasing cooling rate, Figure 11. The crystallinity is lower at higher cooling rates, as will be shown later, and resulting in a smaller crystallization strain. Although less stress relaxation and hence higher curvatures are expected at higher cooling rates, the data indicates that the crystallization shrinkage dominates.

Changes in the process temperature, T_p, did not produce any significant change in the average curvature, Table 6. Due to the amount of scatter in the data, the effects of processing pressure, P_p, are not conclusive, Figure 11.

An unexpected result of high cooling rates was the development of in-plane and out-of-plane fiber microbuckling in the cross-ply laminates. Although wrinkling is a common occurrence in thermoforming with thermoplastics [26,67,68], fiber microbuckling has not been widely reported in unidirectional or cross-ply laminates. Figure 12 shows the microbuckling observed in a $[0_3/90_3]$ 25.4 mm x 152.4 mm APC-2 specimen cooled at a rate of 462°C/min. Similar processing work [69] has shown that for large specimens (e.g. 5 mm x 203 mm x 305 mm panels) microbuckling is present at all cooling rates including rates as low as 0.54°C/min. Grossman and Amateau [5] have shown microbuckling in APC-2 to be a probable cause for the decrease in longitudinal and transverse moduli with increasing cooling rate.

TABLE 6. Characteristics of As-Processed APC-2 Specimens.

Specimen ID	Process Cooling Rate (°C/min)	Wt. % Crystallinity (%)	Dimensionless Curvature (x 10^-4)				
			t1/R1*	t2/R2*	t3/R3*	Average	Standard Deviation
C1112A-1	0.54	32 (d)	55.02	33.01	54.70	47.58	10.30
C1112B-1	0.54	42 (d)	56.31	64.24	62.60	61.05	3.42
C1112C-1	0.54	34 (d)	64.03	60.54	42.66	55.74	9.36
C2112A-1	100.00	24 (d)	54.12	-	24.43	39.28	14.85
C2112B-1	54.14	28 (d)	36.12	41.23	41.72	39.69	2.53
C2112C-1	59.16	31 (d)	49.28	52.74	46.22	49.42	2.67
C2112D-1	74.88	18 (d)	37.67	32.56	32.84	34.36	2.34
C1212A-1	0.54	43 (d)	47.34	52.47	54.02	51.28	2.85
C1212A-2	0.54	43 (d)	52.92	60.06	61.33	58.10	3.70
C1312A-1	0.54	43 (d)	-	69.19a	-	61.19a	0.00
C1312A-2	0.54	43 (d)	-	60.56a	-	60.56a	0.00
C1312B-1	0.54	35 (d)	52.96	59.06	47.76	53.26	4.62
C1312B-2	0.54	28.95	62.38	68.70	61.03	64.04	3.34
C1312C-1	0.54	42.54	49.54	59.14	62.46	57.05	5.48
C1312C-2	0.54	39.50	50.90	52.07	52.39	51.79	0.64
C1312D-1	0.54	30.16	36.35	53.39	47.79	45.84	7.09
C1312D-2	0.54	30.62	56.20	66.98	63.13	62.11	4.46
C1322A-1	0.54	35 (d)	25.90	61.84	64.45	50.73	17.59
C1322A-2	0.54	38 (d)	35.77	65.36	61.25	54.13	13.09
C1322B-1	0.54	40 (d)	45.30	61.89	64.57	57.25	8.52
C1322B-2	0.54	43 (d)	60.75	61.58	57.78	60.03	1.63

TABLE 6. (Continued).

Specimen ID	Process Cooling Rate (°C/min)	Wt. % Crystallinity (%)	Dimensionless Curvature (x 10^-4)				
			t1/R1*	t2/R2*	t3/R3*	Average	Standard Deviation
C2312A-1	89.94	33.90	50.27	46.15	45.40	47.27	2.14
C2312A-2	89.94	33.90	56.14	49.91	46.10	50.72	4.14
C2312B-1	62.26	33.90	43.01	45.26	36.57	41.61	3.68
C2312B-2	62.26	33.90	54.39	57.47	53.15	55.01	1.81
C2312C-1	(b)	29.07	50.98	50.01	49.96	50.32	0.47
C2312D-1	73.67	32.91	53.48	54.57	47.45	51.83	3.13
C2312E-1	57.09	32.59	46.92	46.61	45.97	46.50	0.39
C2312F-1	74.33	35.50	55.06	55.47	40.57	50.37	6.93
C3312A-1	(c)	NA	60.78	68.26	61.70	63.58	3.33
C3312A-2	(c)	NA	54.62	67.42	55.93	59.32	5.75
C3312B-1	312.00	29.68	44.84	50.65	42.81	46.10	3.32
C3312B-2	312.00	29.68	49.40	42.14	27.85	39.80	8.95
C3312C-1	462.00	29.41	44.04	48.57	43.98	45.53	2.15
C3312C-2	462.00	29.41	48.64	56.31	56.01	53.66	3.55
C3312D-1	747.60	28.52	47.94	53.33	51.75	51.00	2.26
C3312D-2	747.60	30.10	45.52	52.92	50.89	49.77	3.12
C3312E-1	318.40	31.58	36.77	41.94	38.35	39.02	2.16
C3312E-2	318.40	31.58	41.67	45.63	46.91	44.74	2.23
C3312F-1	145.30	30 (d)	51.46	54.07	42.60	49.38	4.91
C3312G-1	164.90	25 (d)	45.16	45.02	34.61	41.60	4.94
C3312H-1	870.51	26.13	29.50	46.76	47.79	41.35	8.39
C3312I-1	691.67	30.94	45.70	52.51	47.58	48.60	2.87
C3312J-1	717.30	29.12	46.71	52.21	42.73	47.22	3.88
C3312K-1	377.71	37.67	46.95	57.97	46.40	50.44	5.33
C3312L-1	332.74	39.35	51.63	53.69	47.92	51.08	2.39
C3312M-1	537.94	35.97	50.19	59.57	47.62	52.46	5.14
C3312N-1	415.26	34 (d)	54.99	57.93	45.81	52.91	5.16

* t1/R1, t2/R2, and t3/R3 measured at 114 mm, 76 mm, and 38 mm from TC end of specimen, respectively. All radii determined with a reference block of C = 51 mm. See Figure 5.
(a) Only one radius measured: reference block is C = 127 mm.
(b) Data lost due to computer power failure.
(c) Incomplete consolidation.
(d) Estimated from the literature [75] and Figure 35.

TABLE 7. Effect of Thermal Cycling on Stress-Free Temperature.

Specimen ID	Stress-Free Temperature (Heating/Cooling) (°C)			Mass FractionCrystallinity, Mc (%)				Dimensionless Curvature, t/R (x 10^-4)			
	1 Cycle	2 Cycles	3 Cycles	Before	1 Cycle	2 Cycles	3 Cycles	Before	1 Cycle	2 Cycles	3 Cycles
SF1312B-2	323/323	-	-	28.95	28.46	-	-	68.70	82.61	-	-
SF1312C-1(b)	326/ -	-	-	42.54	NA	-	-	59.14	67.86	-	-
SF1312C-2	324/331	-	-	39.50	29.76	-	-	52.87	64.21	-	-
SF1312D-1(b)	327/ -	-	-	30.16	NA	-	-	53.34	57.59	-	-
SF1312D-2	304/312	-	-	30.62	25.53	-	-	66.98	76.18	-	-
SF2312C-1(b)	283/ -	-	-	29.07	39.40	-	-	50.01	56.40	-	-
SF2312D-1(b)	284/ -	-	-	32.91	NA	-	-	54.57	67.42	-	-
SF2312E-1	279/290	288/320	319/312	32.59	NA	42.82	29.62	46.61	61.29	74.50	72.82
SF2312F-1	300/330	-	-	35.50	33.04	-	-	54.47	86.12	-	-
SF3312D-1	300/327	-	-	28.52	NA	-	-	53.37	74.77	-	-
SF3312D-2	267/329	324/327	-	30.10	37.05	NA	-	52.91	73.08	77.04	-
SF3312H-1(b)	(a)	-	-	26.13	35.76	-	-	41.35	45.63	-	-
SF3312I-1(b)	274/ -	-	-	30.94	36.49	-	-	52.51	62.32	-	-
SF3312J-1(b)	270/ -	-	-	29.12	37.37	-	-	52.21	78.49	-	-

(a) Specimen did not reach stress-free temperature due to temperature controller error.
(b) Phase I testing.

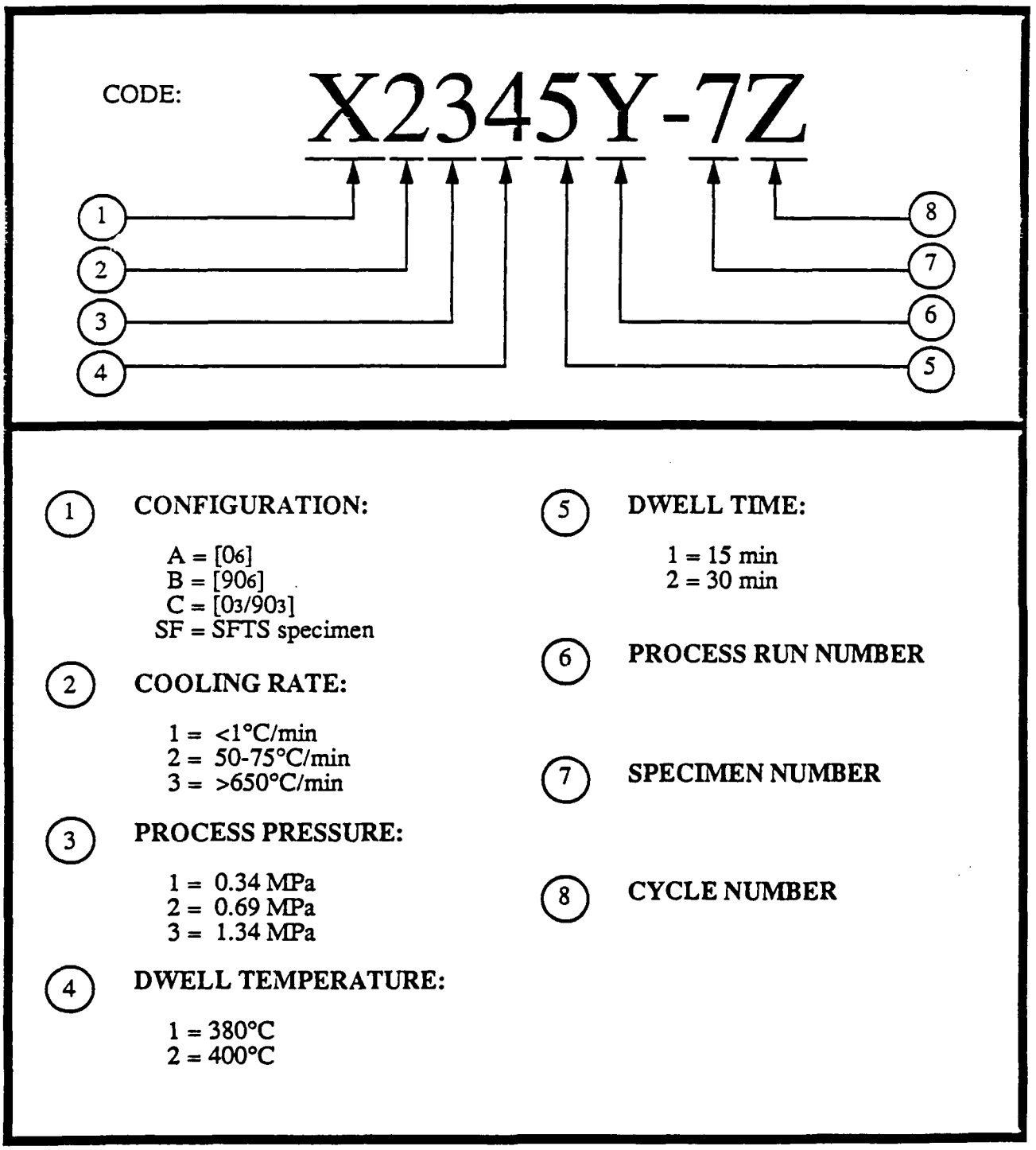

Figure 10. Process Specimen Identification Code.

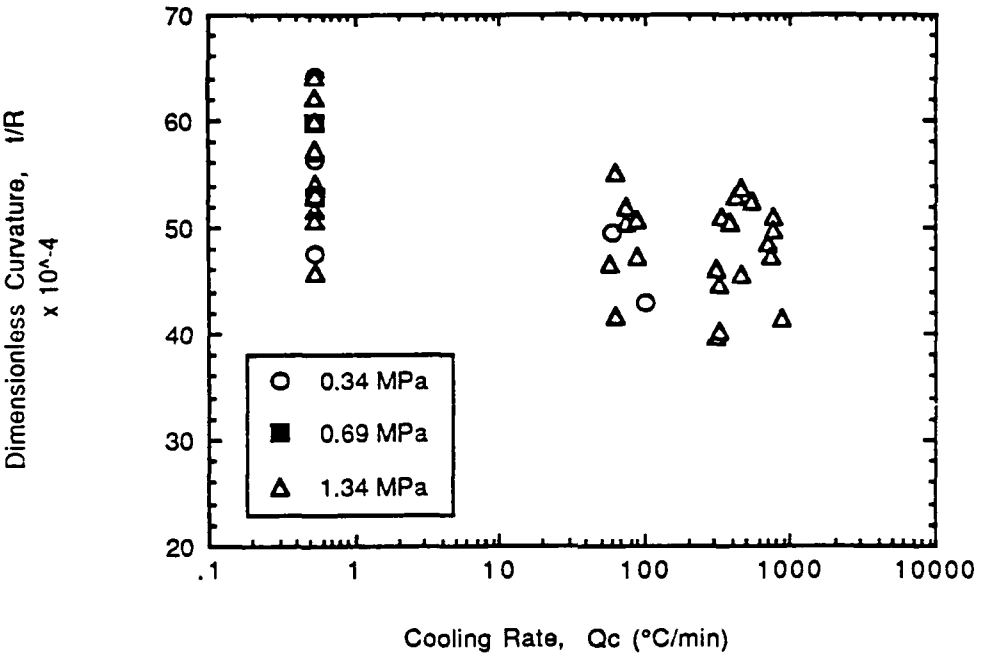

Figure 11. APC-2 Dimensionless Curvature Changes with Process Cooling Rate (Specimen Configuration: $[0_3/90_3]$ 25.4 mm x 152.4 mm).

Microbuckling was found to be a localized phenomenon which could occur for a few number of fibers (1 to 20) or for a large number of fibers (>200). The largest continuous microbuckled area (approximately 3 mm wide and 51 mm long) was found in a $[\pm 45/0_2/90/0_2/\pm 45/0]_s$ 203 mm x 305 mm APC-2 panel cooled at 0.54°C/min. Fiber microbuckling in unidirectional composites due to shrinkage during cure [70] has been reported to remain in phase for fiber separations up to 10 fiber diameters (see Figures 13a and 13b). Only at very large separation of 50 or more fiber diameters do they buckle independently as shown in Figure 13c. The formation, prevention, and effects on mechanical properties of fiber microbuckling is an area that deserves additional investigation.

5.2 Effect of Thermal Cycling on Stress-Free Temperature

The stress-free temperature (SFT) study was carried out in two phases. In Phase I specimens were heated at 3° ± 0.5°C/min until they became flat and then immediately cooled as

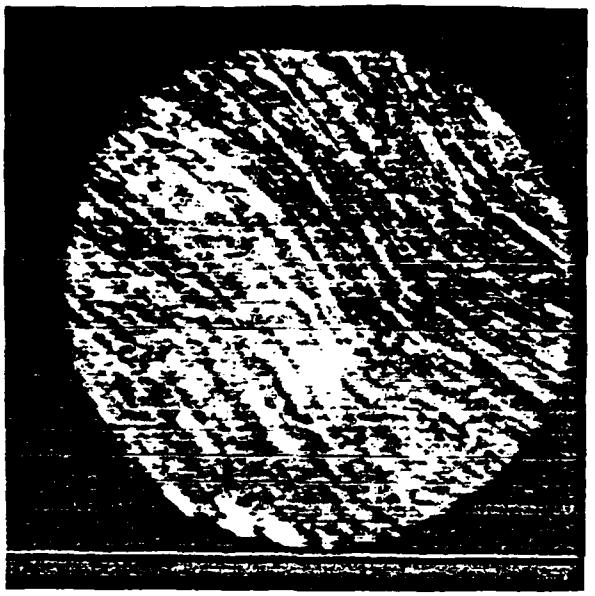

Figure 12. In-Plane and Out-of-Plane Fiber Microbuckling Observed in $[0_3/90_3]$ 25.4 mm x 152.4 mm APC-2 Specimens at High Cooling Rates (Specimen: C3312C-1, Magnification: 21X) [69].

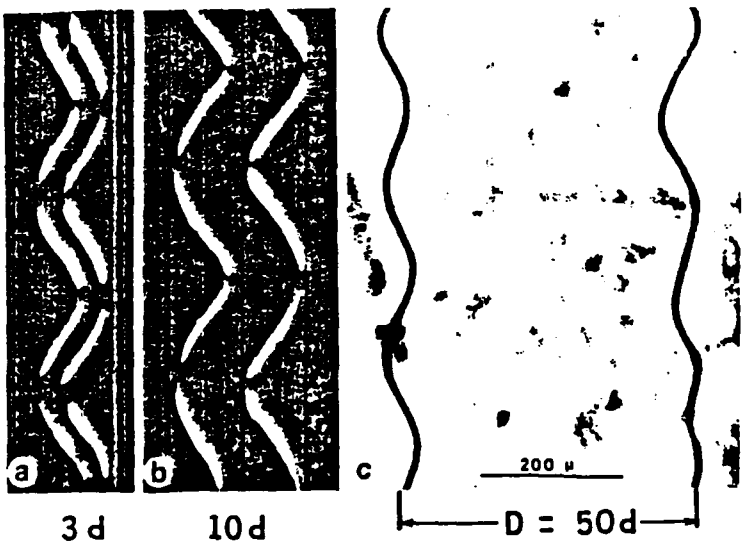

Figure 13. Microbuckling of Fibers in Unidirectional Composites Due to Shrinkage During Curing [70].

quickly as possible. Thus, the maximum temperature reached was a stress-free temperature, which varied from specimen to specimen. The specimens were neither held at the SFT for any length of time nor taken to temperatures higher than the SFT. The purpose of this procedure was to find the SFT associated with the as-processed residual stresses, minimize additional crystallization, and to determine the increase or decrease in the resulting room temperature curvatures after thermal cycling.

In Phase II, the heating and cooling rates were 3°C/min and 1° ± 0.5 °C/min, respectively. The temperature controller was programmed to dwell at 340°C for 15 min before cooling. This was to insure that all specimens were flat and cooled down from the same temperature. Note that in both Phase I and II specimens were left free to deform.

Three distinct SFTs were found for Phase I specimens depending on the process cooling rate. The SFT decreases as the process Q_c increases as shown in Figures 14 through 19. Upon cooling all but one specimen experienced a 9 to 24% increase in dimensionless curvature compared with the as-processed curvature. The exception was specimen SF3312J-1 which showed a much higher increase. During processing the specimens were held flat by the mold, and hence free curvature development was not allowed. The increase in curvatures is thus believed to be the result of an absence of geometric constraints on the specimen and is seen to be a function of the amount of time spent in the crystalline temperature range (180°-320°C) and the previous temperature history of the specimen. In the case of specimen SF3312J-1, which was processed at a cooling rate of 717°C/min, its mass fraction crystallinity (M_c) was a low 29% making it a prime candidate for additional crystallization during the thermal cycling. The M_c of SF3312J-1 increased by 28% after one SFT cycle as shown in Table 7. Therefore, the increase in t/R can be explained by additional strain due to crystallization.

As mentioned earlier, all Phase II specimens were heated to 340°C during thermal cycling. All specimens became flat before reaching the maximum temperature of 340°C. Upon cooling different specimens began to show curvature development at different temperatures. Thus, two stress-free temperatures were measured during each thermal cycle: a heating SFT and a cooling SFT.

The low Q_c (< 1°C/min) specimens had a heating and cooling SFT that were very close to each other as shown in Table 7 and illustrated in Figures 20 through 22. The heating and cooling curves for the medium or normal cooling rate (50°-75°C/min) are shown in Figures 23 and 24. Specimen SF2312E-1 was cycled 3 times using the same thermal cycle. Starting out with a low

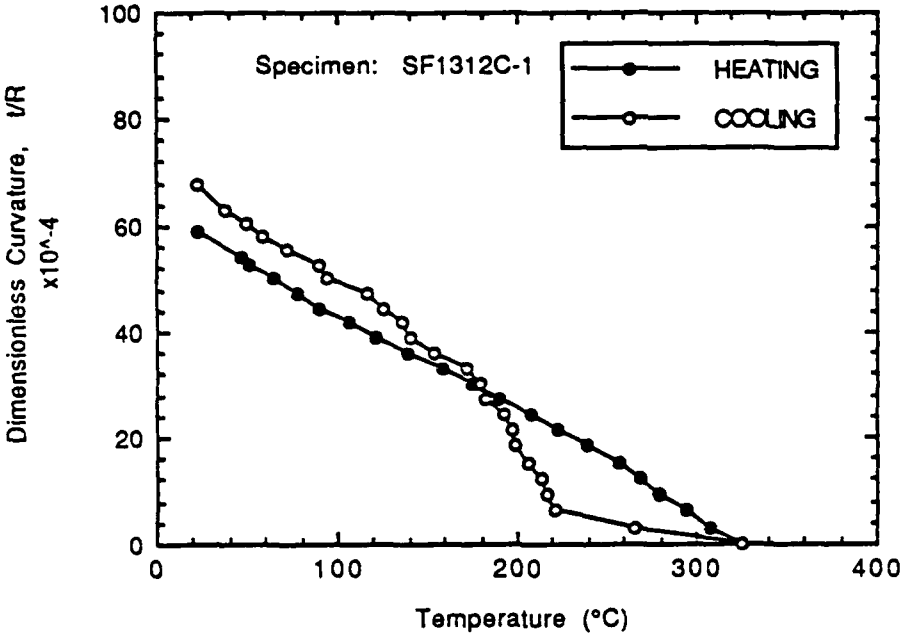

Figure 14. Dimensionless Curvature for a Single SFT Cycle, Phase I, of a $[0_3/90_3]$ Specimen Processed at a Cooling Rate of 0.54°C/min (SFT=326°C).

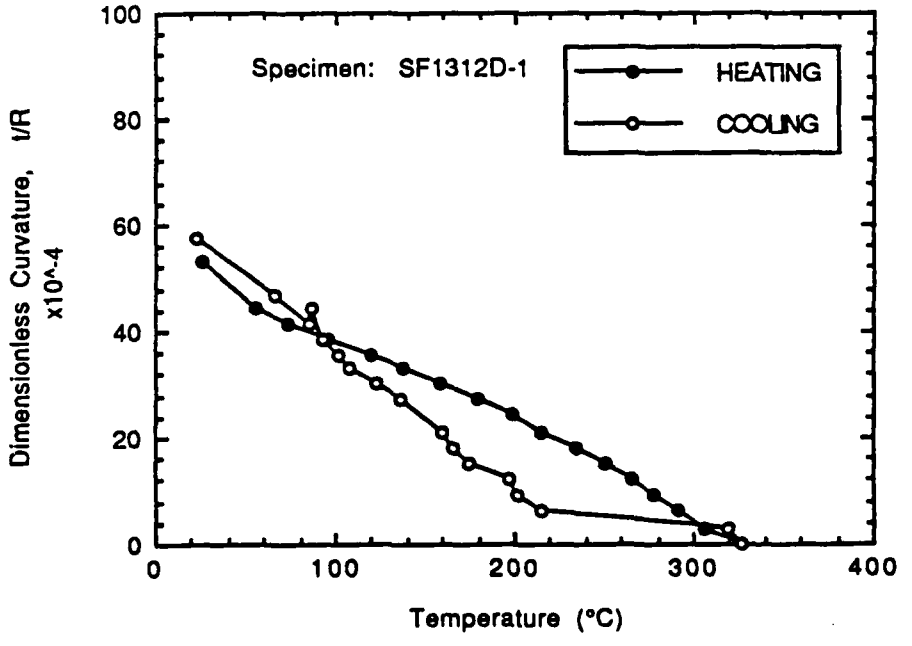

Figure 15. Dimensionless Curvature for a Single SFT Cycle, Phase I, of a $[0_3/90_3]$ Specimen Processed at a Cooling Rate of 0.54°C/min (SFT=327°C).

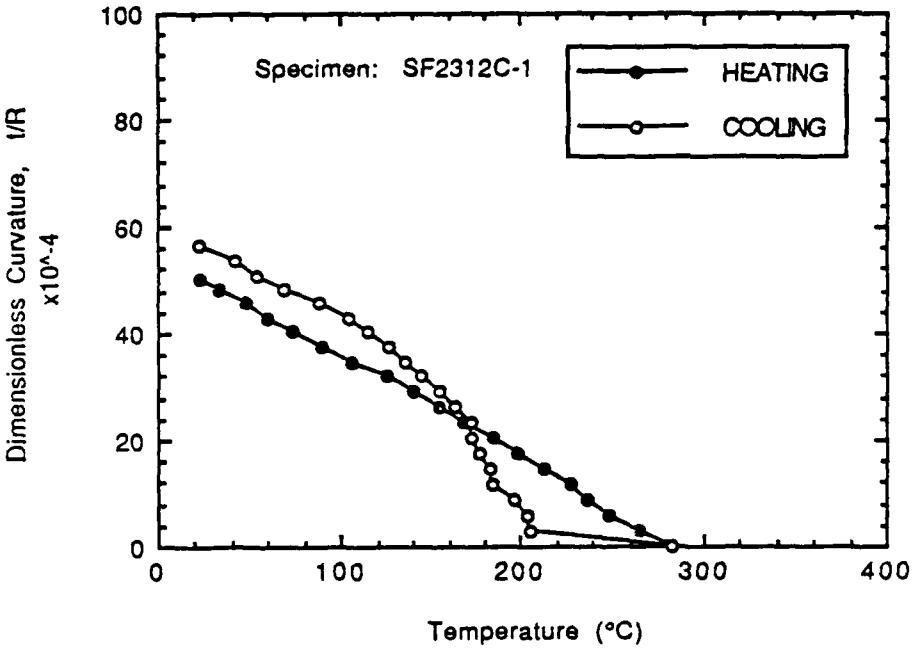

Figure 16. Dimensionless Curvature for a Single SFT Cycle, Phase I, of a $[0_3/90_3]$ Specimen Processed at a Cooling Rate of ~60°C/min (SFT=283°C).

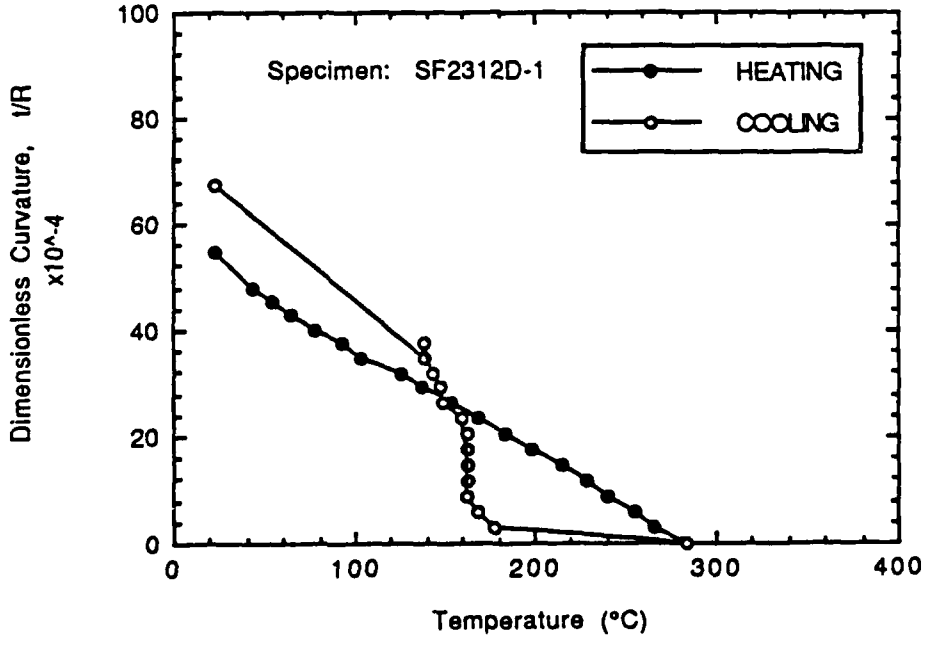

Figure 17. Dimensionless Curvature for a Single SFT Cycle, Phase I, of a $[0_3/90_3]$ Specimen Processed at a Cooling Rate of 74°C/min (SFT=284°C).

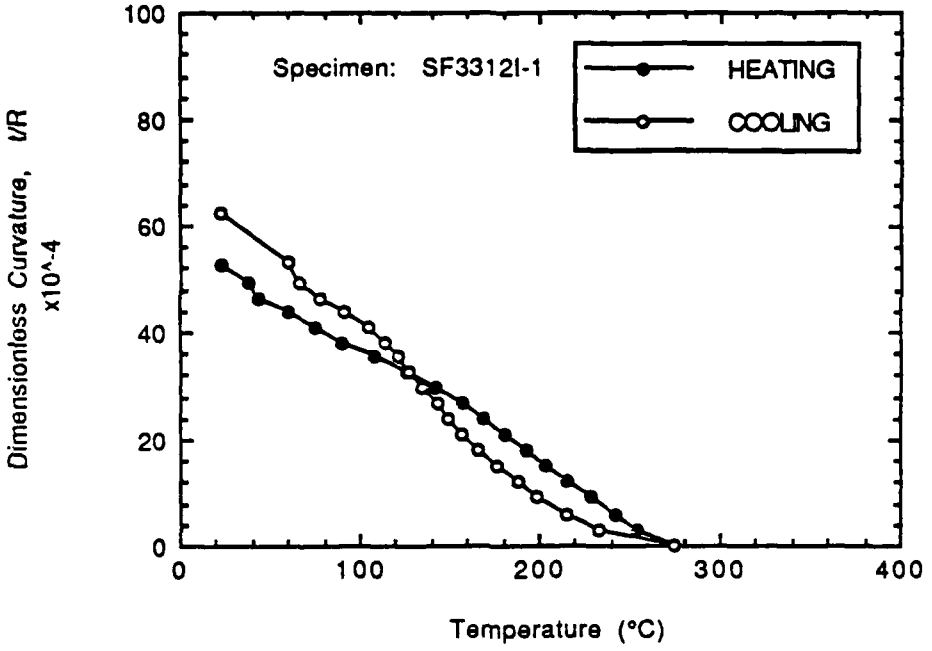

Figure 18. Dimensionless Curvature for a Single SFT Cycle, Phase I, of a $[0_3/90_3]$ Specimen Processed at a Cooling Rate of 692°C/min (SFT=274°C).

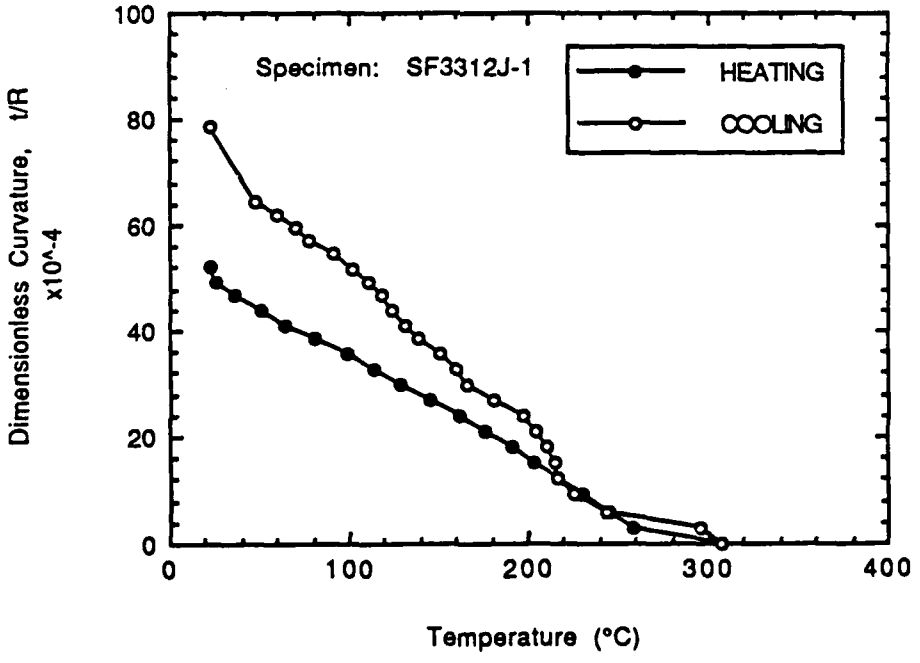

Figure 19. Dimensionless Curvature for a Single SFT Cycle, Phase I, of a $[0_3/90_3]$ Specimen Processed at a Cooling Rate of 717°C/min (SFT=270°C).

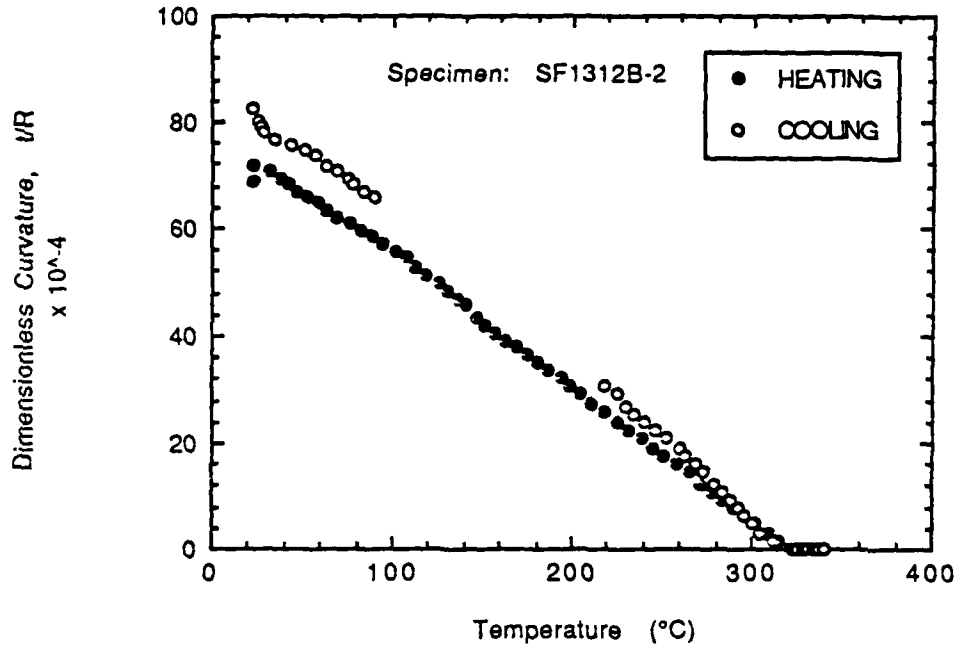

Figure 20. Dimensionless Curvature for a Single SFT Cycle, Phase II, of a $[0_3/90_3]$ Specimen Processed at a Cooling Rate of 0.54°C/min (SFT=323°C).

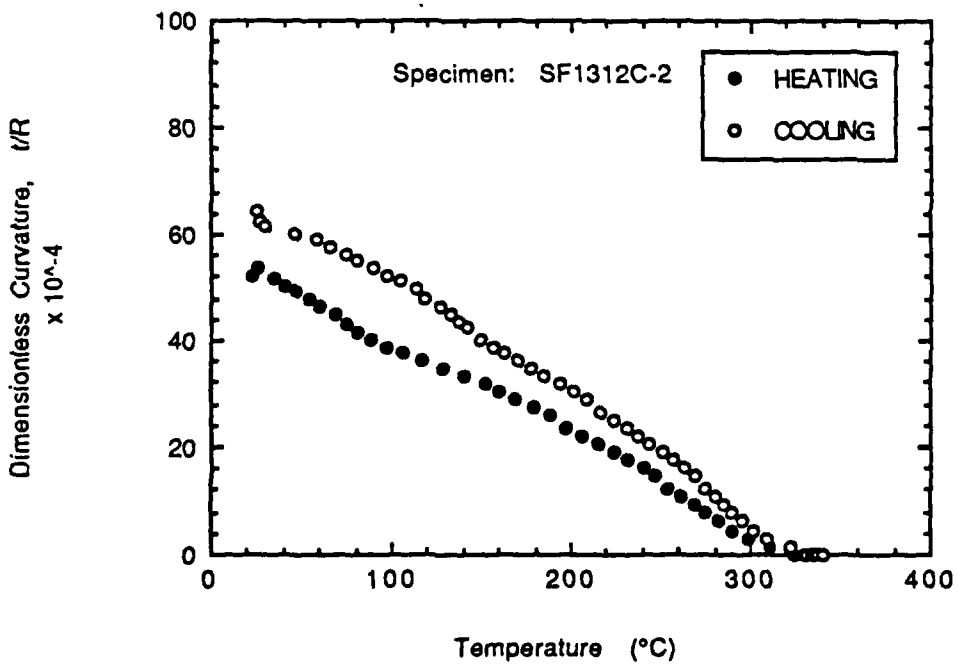

Figure 21. Dimensionless Curvature for a Single SFT Cycle, Phase II, of a $[0_3/90_3]$ Specimen Processed at a Cooling Rate of 0.54°C/min (SFT=331°C).

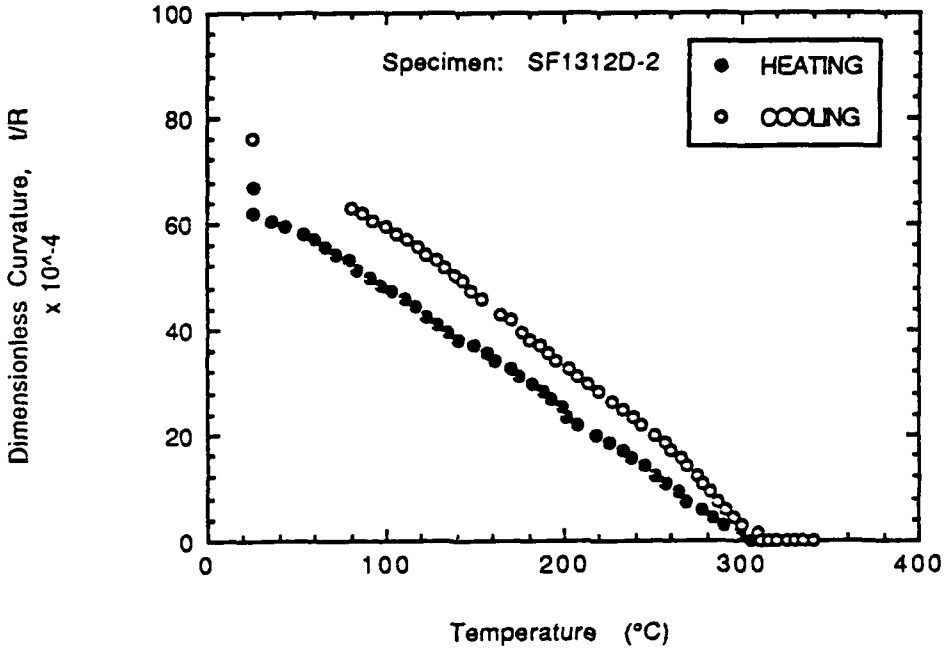

Figure 22. Dimensionless Curvature for a Single SFT Cycle, Phase II, of a $[0_3/90_3]$ Specimen Processed at a Cooling Rate of 0.54°C/min (SFT=312°C).

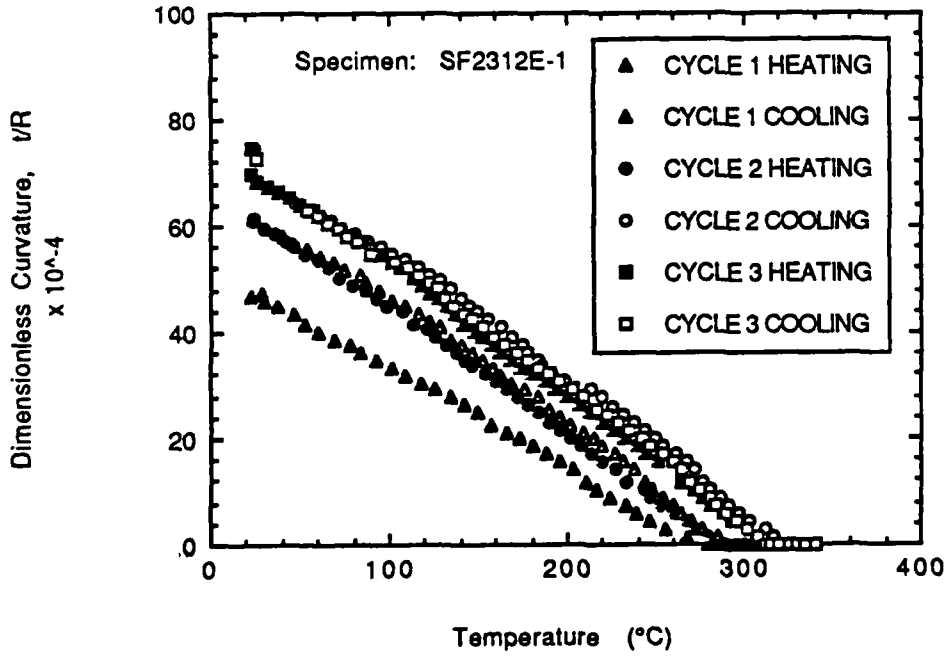

Figure 23. Cycling Dependence of the Dimensionless Curvature for a $[0_3/90_3]$ Specimen Processed at a Cooling Rate of 57°C/min (SFT=290°, 320°, 312°C).

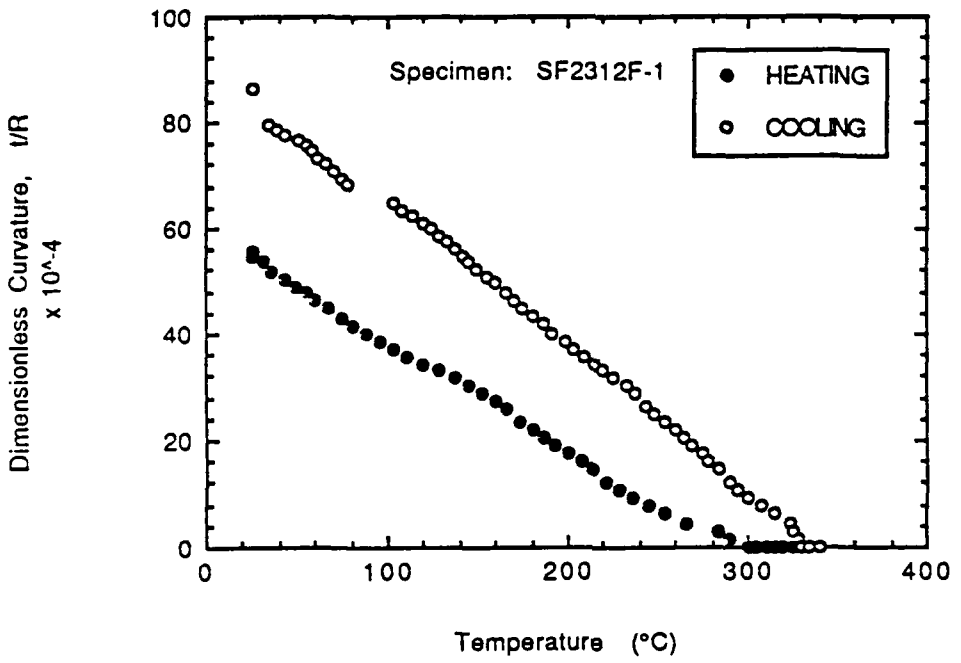

Figure 24. Dimensionless Curvature for a Single SFT Cycle, Phase II, of a $[0_3/90_3]$ Specimen Processed at a Cooling Rate of 74°C/min (SFT≈330°C).

t/R (46.61) and a moderate M_c (32.59%), the specimen achieved a heating SFT of 279°C and a cooling SFT of 290°C. Note in Figure 23 that on successive heating and cooling, the heating curve always follows the previous cooling curve indicating additional crystallinity change and stress relaxation during heating is negligible. Once the specimen became flat it remained so even under increasing temperature. In Phase I the temperature at which curvature began to develop was the same as the maximum temperature reached. However, when cooled from 340°C the curvature did not develop until 320°C was reached. The final cooling curve resembles that of the low Q_c specimens. The inflections at 140°C are seen only in a few of the cooling curves while remaining curves are featureless and linear,as observed with Gr/J Polymer and Gr/PEEK (APC-1) [25].

High Q_c (>650°C/min) specimens also exhibited similar heating and cooling behavior, Figures 24 and 25. Again, SFT's of both specimens increased to about 328°C after they had been heated to 340°C.

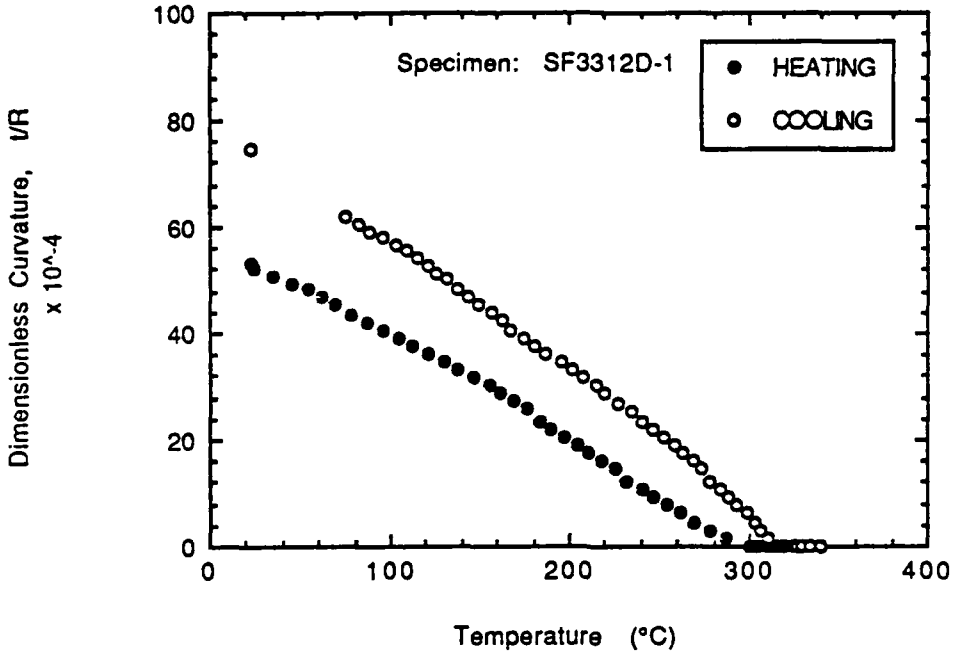

Figure 25. Dimensionless Curvature for a Single SFT Cycle, Phase II, of a $[0_3/90_3]$ Specimen Processed at a Cooling Rate of 748°C/min (SFT=327°C).

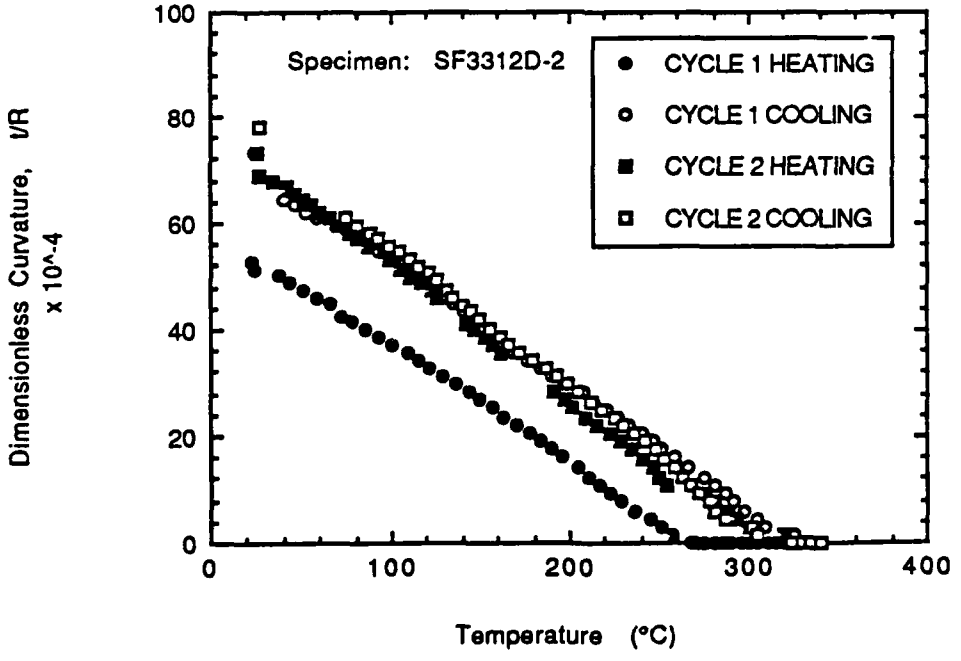

Figure 26. Cycling Dependence of the Dimensionless Curvature for a $[0_3/90_3]$ Specimen Processed at a Cooling Rate of 748°C/min (SFT=329°, 327°C).

The change of room-temperature curvature with SFT cycles in summarized in Figure 27. Here the curvature was measured immediately before the thermal cycling. The curvatures measured after processing decrease with increasing process cooling rate. Higher cooling rates result in lower crystallinity and, hence, lower crystallization shrinkage. In spite of stress relaxation, the net effect is still lower residual stresses for higher cooling rates.

As discussed earlier, the combination of a higher maximum temperature and no geometric constraints imposed during SFT cycling leads to higher curvatures. The curvature increases almost linearly with the subsequently measured stress-free temperature regardless of the process cycle or thermal cycling, Figure 28.

The results for all SFT cycles are summarized in Table 7. The t/R and X_c was measured for each specimen before and after each cycle along with the SFT experienced on both heating and cooling. Figures 29 through 31 show the variations in the SFT cooling curves from specimen to specimen. Figure 32 overlays all t/R cooling curves to develop an upper and lower limit for predicting the amount of residual stresses. It is seen that an asymmetric $[0_3/90_3]$ APC-2 cross-ply laminate with an aspect ratio, L/W, of 6 has a SFT of 320° ± 20°C and a dimensionless curvature of 72 ± 8 (x 10^{-4}) at room temperature after thermal cycling to 340°C regardless of the process cooling rate employed.

The final step of Phase II was to reheat under contact pressure a representative specimen from each process Q_c group. This was achieved by placing the specimen back into the mold to prevent warpage and applying the same thermal cycle as in Phase II SFT cycles. The t/R decreased for both the low and medium cooling rate specimens, whereas the high Q_c specimen remained unchanged (Table 8). This is in contrast to the observation described earlier that the curvature increased after thermal cycling when specimens were left free to deform. The main reason for the contrast is that more stress relaxation occurs when the specimen is kept flat, thereby reducing the curvature.

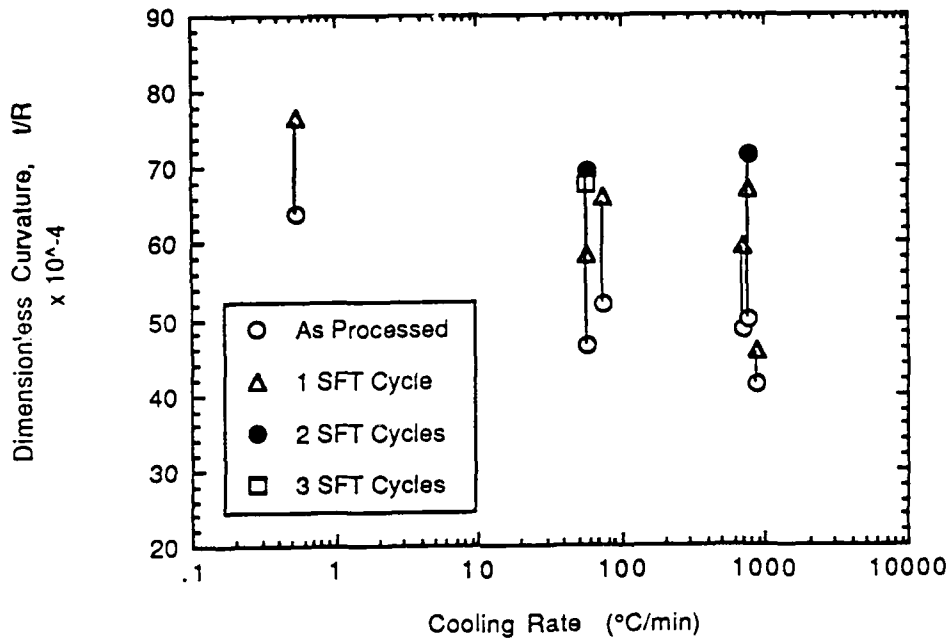

Figure 27. Dimensionless Curvature as a Function of Process Cooling Rates and Thermal Cycling of Phase II APC-2 Specimens.

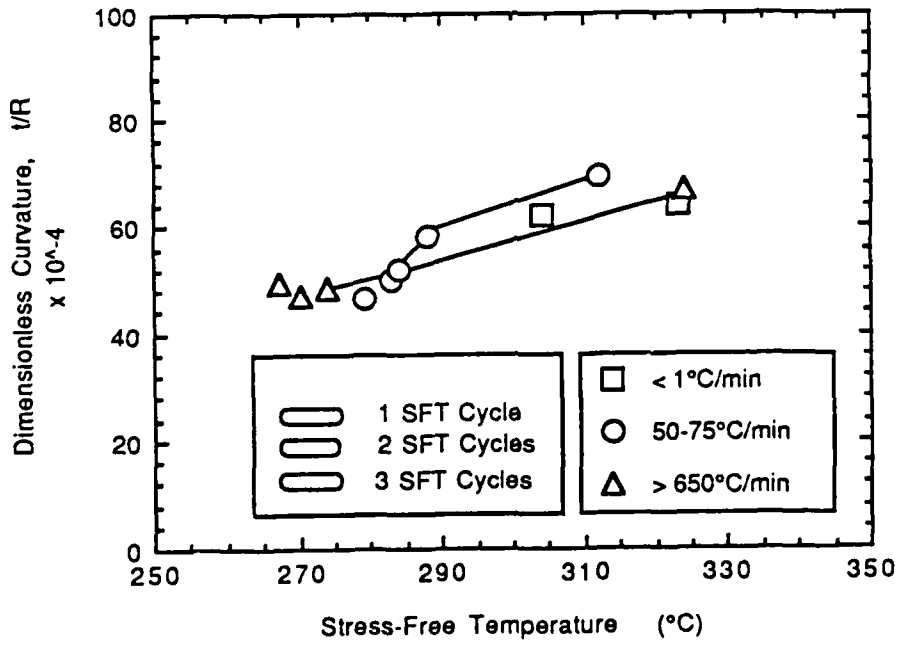

Figure 28. Heating SFT Dependence on Thermal Cycling and Initial Dimensionless Curvature.

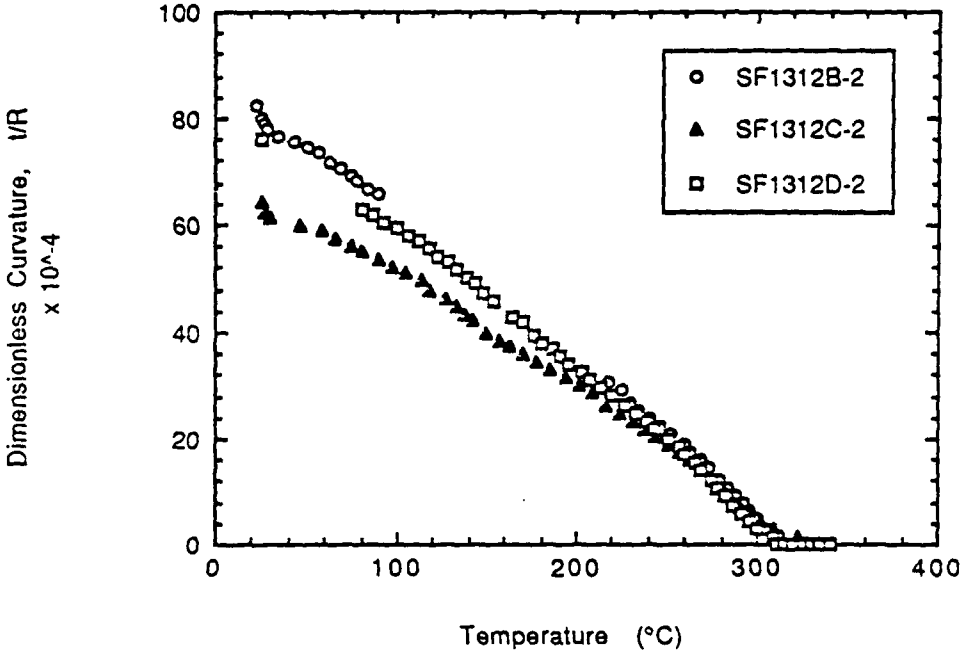

Figure 29. Dimensionless Curvature as a Function of Cool Down Temperatures for Low (< 1°C/min) Process Cooling Rates of Phase II APC-2 Specimens.

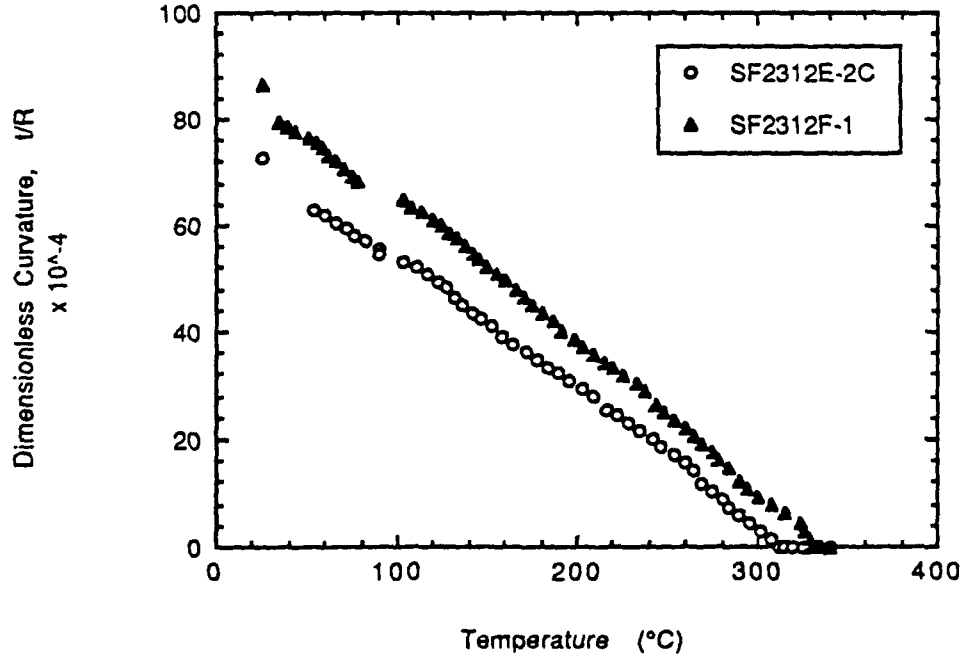

Figure 30. Dimensionless Curvature as a Function of Cool Down Temperatures for Medium (50°-75°C/min) Process Cooling Rates of Phase II APC-2 Specimens.

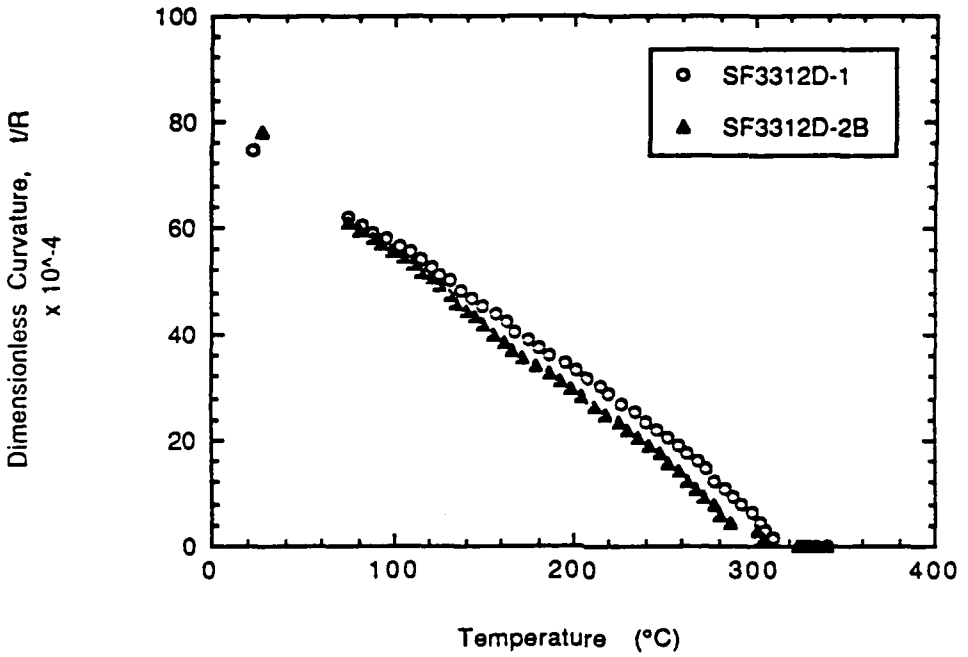

Figure 31. Dimensionless Curvature as a Function of Cool Down Temperatures for High (> 650°C/min) Process Cooling Rates of Phase II APC-2 Specimens.

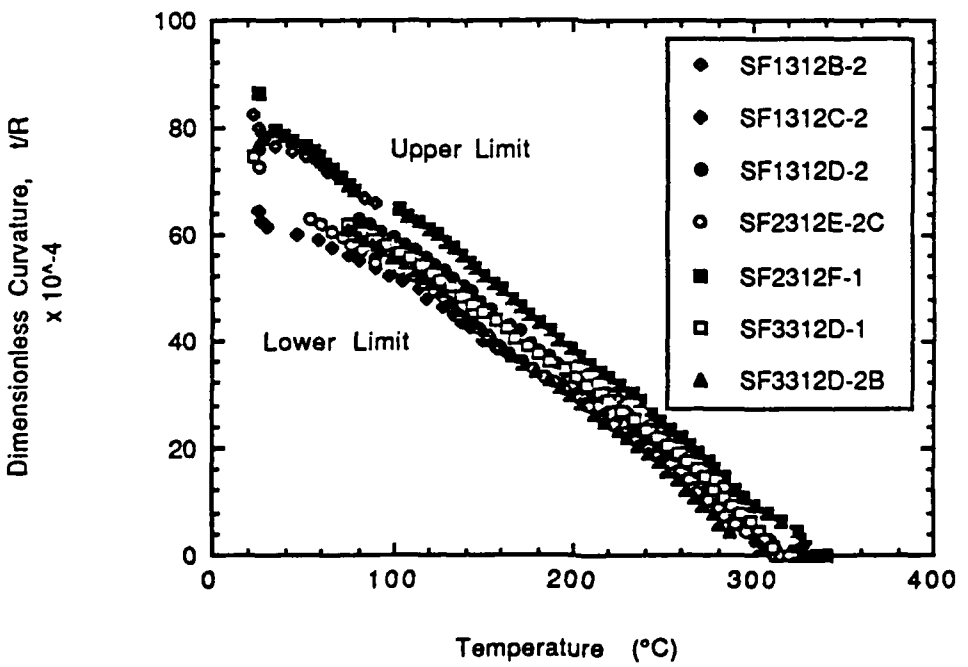

Figure 32. Upper and Lower Limits of Dimensionless Curvature During Cool Down of Phase II APC-2 Specimens.

TABLE 8. Effect of Geometric Constraint on Curvature During Thermal Cycling.

Specimen ID	Process Cooling Rate (°C/min)	Dimensionless Curvature (x 10^-4)	
		Before	After
C1312B-1	0.54	55.12 ± 5.78	46.35 ± 6.17
C2312B-1	62.26	42.16 ± 2.54	33.94 ± 2.89
C3312C-2	462.00	54.84 ± 3.07	55.47 ± 5.89

5.3 Crystallinity Study

The mass fraction crystallinity was measured during heating by differential scanning calorimetry (DSC) for several specimens after processing [5,48,71]. A typical DSC run is shown in Figure 33 where the specimen was heated at 10°C/min to 380°C, held there for 15 min, then cooled at 60°C/min. From this trace we can see that the onset of melting is 330°C with a melt temperature of 343°C. Using Eq. (3) we find M_c to be 37.81%.

The exotherm due to crystallization during cooling at 1°C/min and 60°C/min are shown in detail in Figures 34 and 35, respectively. The onset of crystallization (T_{oc}) is seen to decrease with increasing Q_c and the crystallization range from T_{oc} to T_{ec}, the end of crystallization temperature, broadens with increasing Q_c. The SFT was found to coincide with the T_{oc} as had been observed with other semi-crystalline thermoplastics [25]. The resulting crystallinities are 37.1% and 31.5% for 1°C/min and 60°C/min cooling, respectively. The results for as-processed and thermal cycled specimens are given in Tables 6 and 7, respectively.

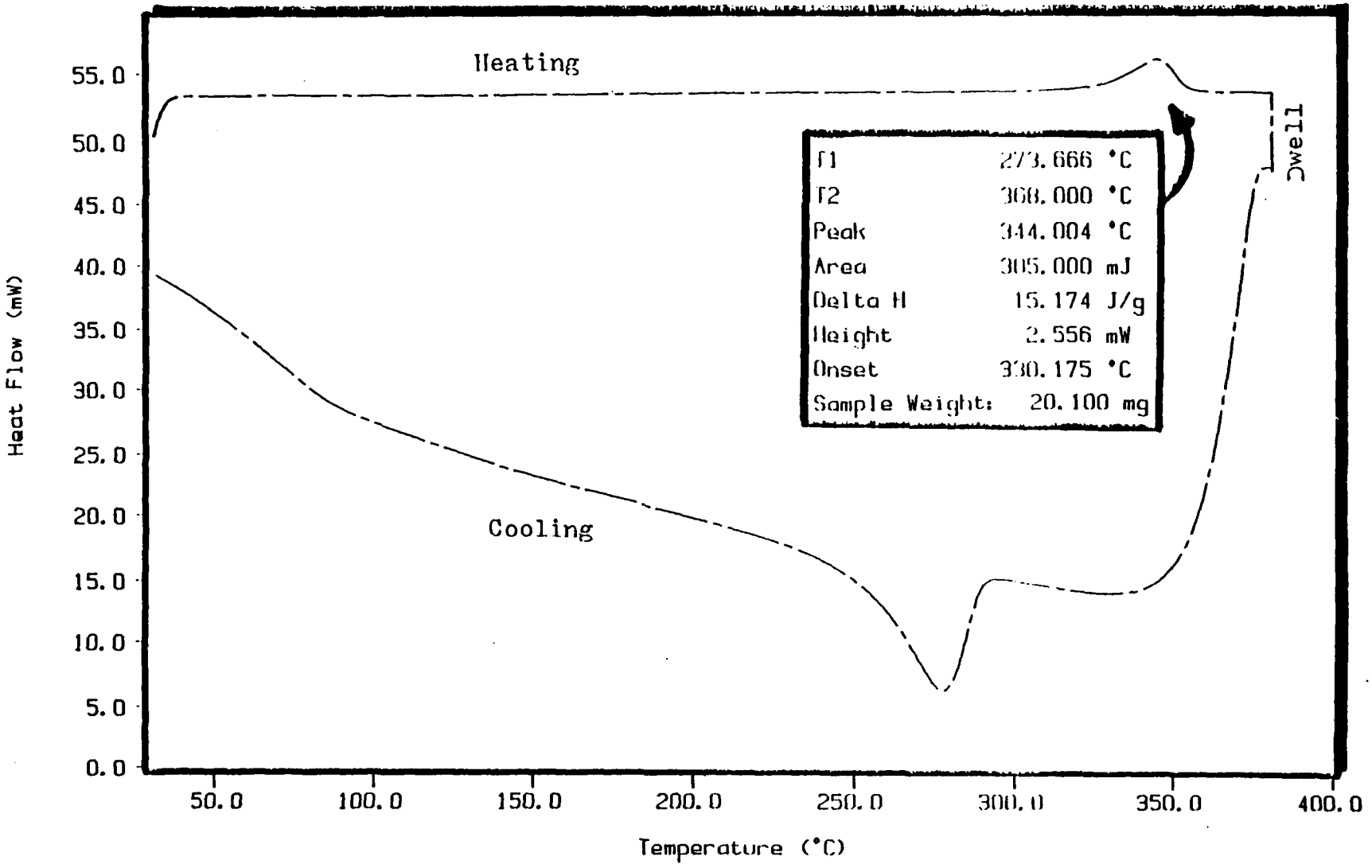

Figure 33. DSC Trace for a [0_3/90_3] APC-2 Composite (Heating: 10°C/min, Dwell: 15min at 380°C, Cooling: 60°C/min; Specimen: C3312K-1).

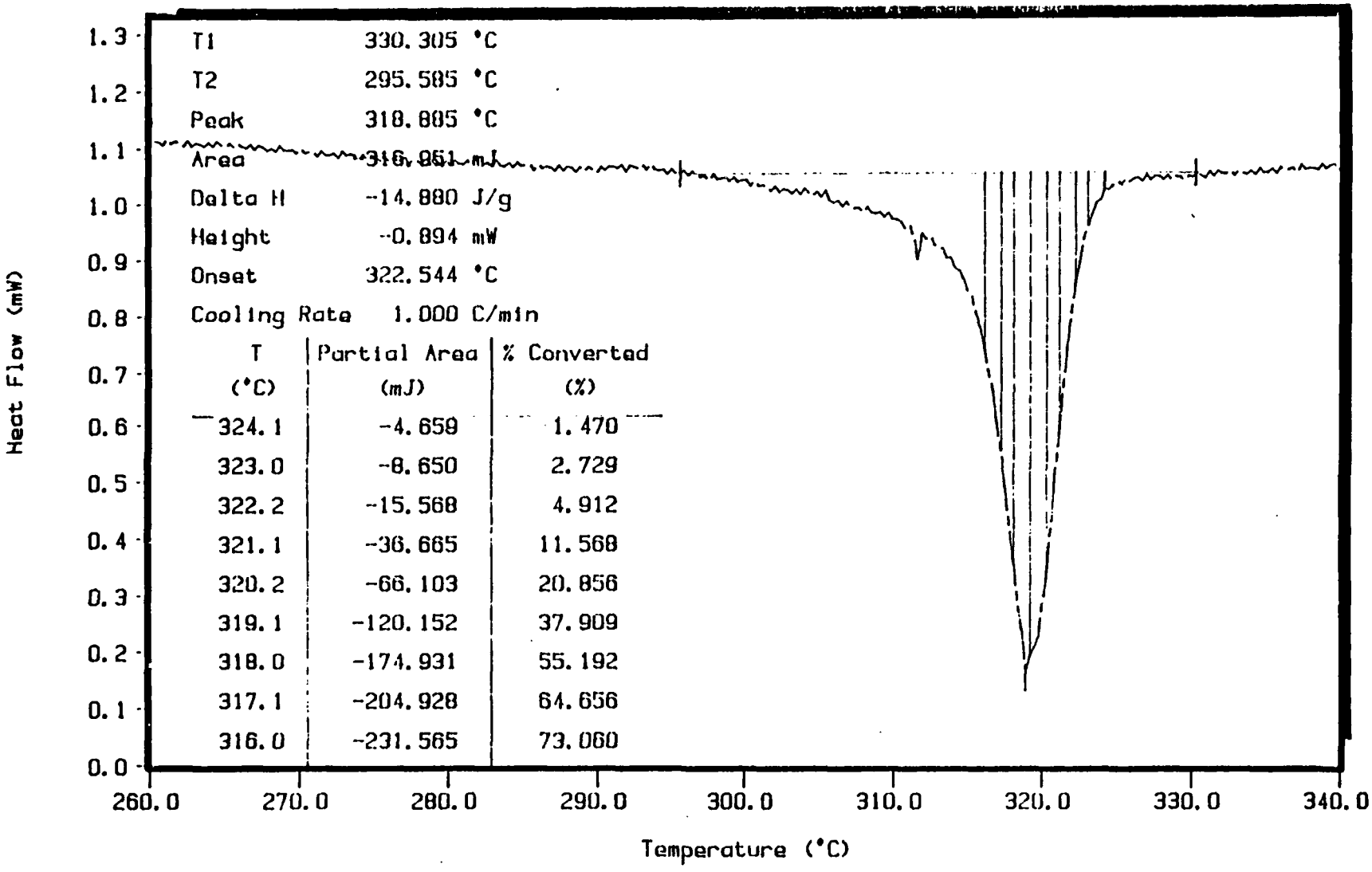

Figure 34. Partial Integration of Area Under Exotherm Curve for 1°C/min Cooling (Specimen: C2312E-1).

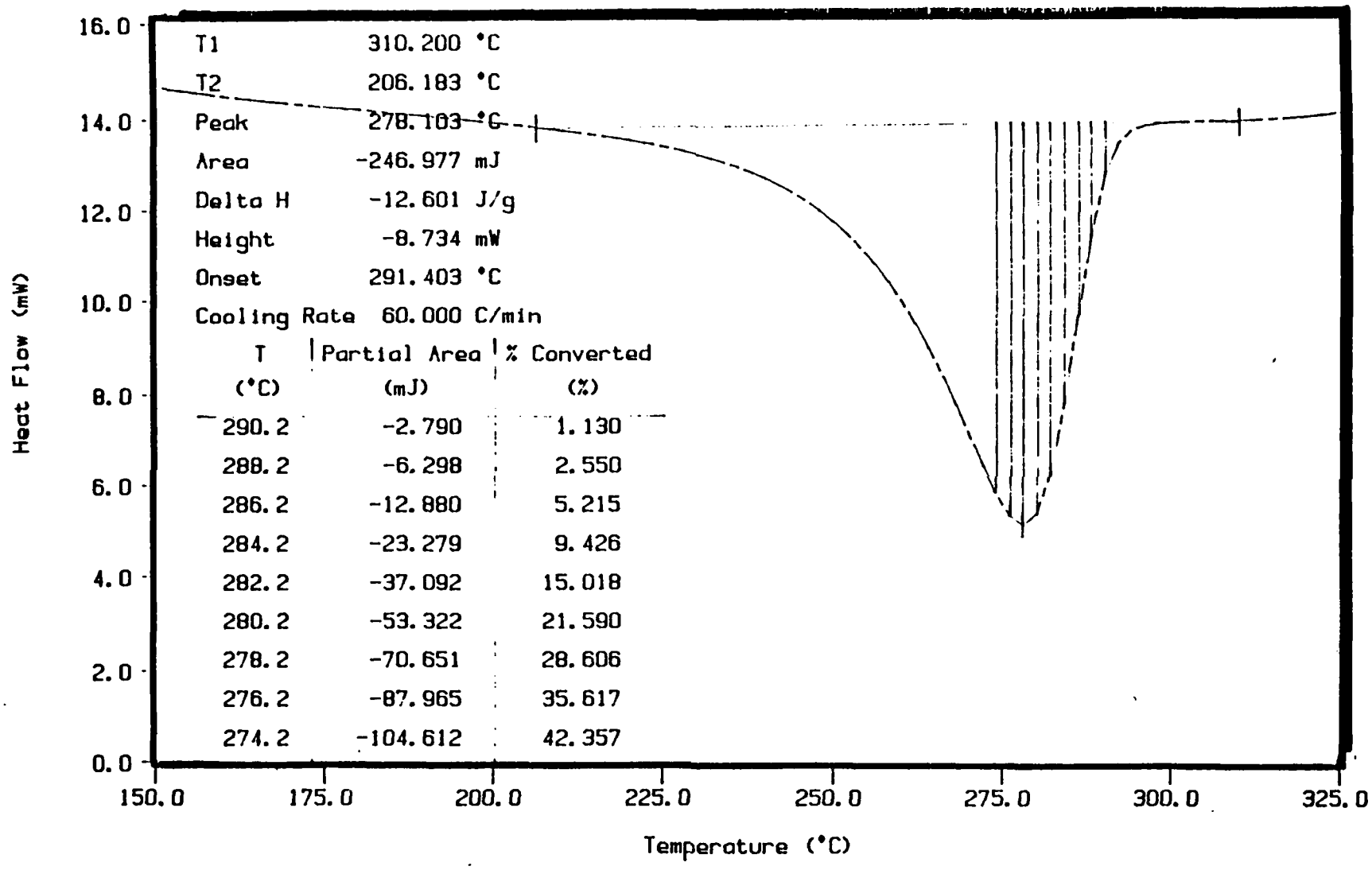

Figure 35. Partial Integration of Area Under Exotherm Curve for 60°C/min Cooling (Specimen: C2312E-1).

DSC testing at the same thermal cycle parameters as Phase II SFT specimens was performed to calculated the amount of additional crystallization for the selected thermal cycle. The results showed that heating of APC-2 to 340°C with a 15 minute dwell was insufficient to achieve full melting of the matrix and subsequent cooling at 1°C/min did not produced a noticeable exotherm. Hence, additional crystallization did not take place as expected and the increase in the room temperature curvature must be explained by other means. If the specimen had reached full melt then an exotherm similar to Figure 34 would have occurred and the additional crystallization would account for additional transverse shrinkage and thus, a larger dimensionless curvature.

Figure 36 shows that crystallinity data obtained in the present study under the conditions of T_p = 380°C, Δt_D = 30 min, and P_p = 1.34 MPa compares very well with previously reported results for APC-2. It is important to note that the low or negligible crystallinity reported in the literature [20,36,41,42,48,59,72] for cooling rates of 1,000° to 10,000°C/min were for specimen sizes of 19 mm x 152 mm or smaller processed from a single specimen mold. The molds used in the present work were a 178 mm x 216 mm multi-specimen mold and a 203 mm x 305 mm panel mold. The large size of the present molds made it difficult to achieve high cooling rates.

Crystallinity in several high cooling rate specimens was uniform in the transverse direction, but showed a 38% variation along the longitudinal direction, Table 9. This can be explained by the quench method used for the high Q_c specimens. As seen from Figure 36, a change in the M_c from 24% to 33% requires a change in cooling rate from 300 to 800°C/min. Since the ice/water quench method provides no control for the cooling rate it is likely that the specimens experienced uneven cooling over the length of the specimen. This is also supported by the variation in the dimensionless curvature across the specimens (Table 6).

Plotting the as-processed curvature as a function of M_c (Figure 37) we can see a slight trend in the data. As one would expect from the relationship between t/R vs Q_c and M_c vs Q_c, the dimensionless curvature increases with increasing crystallinity.

5.4 Crystallization Shrinkage

The transverse strain in the matrix due to crystallization, e^c_T, was calculated by integrating the area under the exotherm (Figures 34 and 35) from T_{oc} to T to determine the enthalpy change then using Eq. (15) to find e^c_T (T). The results of this study are listed in Tables 10 and 11. The increase in matrix crystallization strain as a function of temperature and cooling rate is shown in

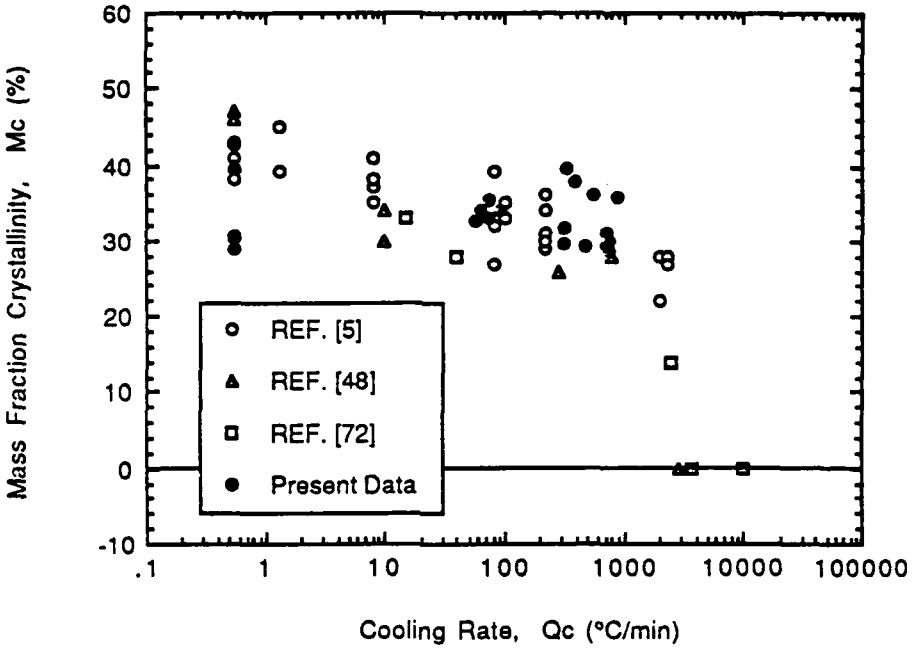

Figure 36. Mass Fraction Crystallinity as a Function of Process Cooling Rate for APC-2.

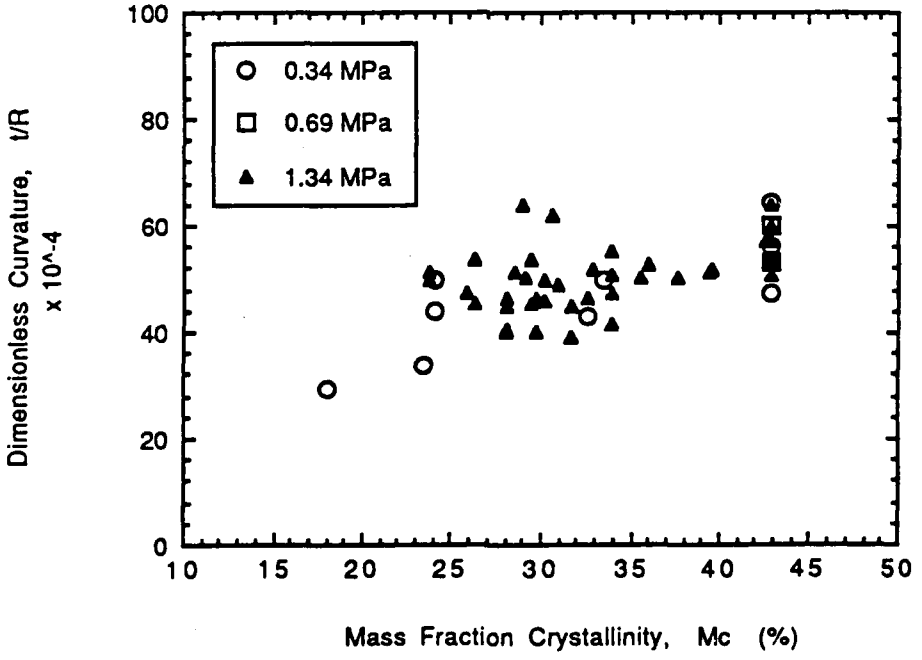

Figure 37. Correlation Between Dimensionless Curvature and Mass Fraction Crystallinity Due to Changes in Processing Pressure.

TABLE 9. Crystallinity Profile of High Cooling Rate Specimens.

Specimen ID	Mass Fraction Crystallinity (%)	Dimensionless Curvature ($\times 10^{-4}$)
A-1	33.25	47.15
B-1	32.91	47.94
C-1	28.52	53.33
F-1	24.14	51.75
F-2	24.41	51.75

TABLE 10. Exotherm Integration for 1°C/min Cooling.[a]

Temperature (°C)	Integrated Area (mJ)	Hc Enthalpy of Crystallization (J/g)	ε^{c}_{T} Transverse Crystalline Strain (%)
329	0.74	0.038	0.0017
328	1.18	0.060	0.0028
327	1.79	0.091	0.0043
326	3.36	0.121	0.0057
325	2.38	0.172	0.0080
324	5.34	0.272	0.0127
323	8.65	0.441	0.0206
322	19.24	0.982	0.0457
321	36.67	1.871	0.0872
320	78.46	4.003	0.1866
319	120.15	6.130	0.2857
318	174.93	8.925	0.4159
317	212.82	10.858	0.5060
316	231.57	11.815	0.5506
315	248.57	12.682	0.5910
314	257.89	13.158	0.6132
313	267.74	13.660	0.6366
312	273.97	13.978	0.6514
311	282.31	14.403	0.6712
310	288.29	14.709	0.6855
309	292.18	14.907	0.6947
308	296.80	15.143	0.7057
307	300.03	15.308	0.7134
306	303.80	15.500	0.7223
305	305.93	15.609	0.7274
304	308.35	15.732	0.7331
303	310.70	15.852	0.7387
302	312.21	15.929	0.7423
301	313.95	16.018	0.7465
300	314.97	16.070	0.7489
299	315.79	16.112	0.7508
298	316.31	16.138	0.7521
297	316.89	16.168	0.7534
296	316.99	16.173	0.7537

(a) Source: C2312E-1, Specimen Wt.: 21.3 mg

TABLE 11. Exotherm Integration for 60°C/min Cooling[a]

Temperature (°C)	Integrated Area (mJ)	Hc Enthalpy of Crystallization (J/g)	ε_T^c Transverse Crystalline Strain (%)
308	0.01	0.000	0.0000
306	0.03	0.001	0.0001
304	0.06	0.003	0.0001
302	0.10	0.005	0.0002
300	0.16	0.008	0.0004
298	0.25	0.013	0.0006
296	0.39	0.020	0.0009
294	0.66	0.033	0.0016
292	1.24	0.063	0.0030
290	2.79	0.142	0.0066
288	6.30	0.321	0.0150
286	12.88	0.657	0.0306
284	23.28	1.188	0.0553
282	37.09	1.892	0.0882
280	53.32	2.721	0.1268
278	70.65	3.605	0.1680
276	87.97	4.488	0.2091
274	104.61	5.337	0.2487
272	120.17	6.131	0.2857
270	134.41	6.858	0.3196
268	147.32	7.517	0.3503
266	158.93	8.109	0.3779
264	169.31	8.638	0.4025
262	178.54	9.109	0.4245
260	186.75	9.528	0.4440
258	194.04	9.900	0.4614
256	200.50	10.229	0.4767
254	206.22	10.521	0.4903
252	211.29	10.780	0.5024
250	215.79	11.009	0.5131
248	219.77	11.213	0.5225
246	223.31	11.393	0.5309
244	226.44	11.553	0.5384
242	229.22	11.695	0.5450

(a) Source: C2312E-1, Specimen Wt.: 19.6 mg

TABLE 11. (Continued).

Temperature (°C)	Integrated Area (mJ)	Hc Enthalpy of Crystallization (J/g)	ε^{c}_{T} Transverse Crystalline Strain (%)
240	231.69	11.821	0.5509
238	233.87	11.933	0.5561
236	235.83	12.032	0.5607
234	237.55	12.120	0.5648
232	239.07	12.198	0.5684
230	240.42	12.266	0.5716
228	241.61	12.327	0.5744
226	242.64	12.380	0.5769
224	243.54	12.426	0.5791
222	244.32	12.465	0.5809
220	244.98	12.499	0.5825
218	245.53	12.527	0.5838
216	245.99	12.551	0.5849
214	246.36	12.569	0.5857
212	246.63	12.583	0.5864
210	246.83	12.593	0.5869
208	246.94	12.599	0.5871
206	246.98	12.601	0.5872

(a) Source: C2312E-1, Specimen Wt.: 19.6 mg

Figure 38. From this plot and Figures 34 and 35 we can see that the maximum crystallization rate occurs at 319°C for 1°C/min cooling and 278°C for 60°C/min cooling. The longitudinal and transverse thermal expansional strains calculated from Eqs. (9) and (10), respectively, are shown in Figure 39 as a function of temperature. Here it can be seen that the transverse thermal strain is three orders of magnitude greater than the longitudinal strain. Because the transverse thermal strain dominates over the matrix crystallization strain and longitudinal thermal strain there is no significant change in the strain difference, $e_L - e_T$, with respect to changes in the process cooling rate, Figure 40.

5.5 Fiber Volume Fraction

Because of the wide range of results reported in the literature for the fiber volume fraction (V_f) of APC-2 (58 to 66%), it was decided to verify the fiber content independently. Ten photomicrographs were taken randomly of various locations of a $[0_6]$ APC-2 cross-section using a standard metallographic microscope at 400X and a scanning laser microscope (SLM) at 500X. Several of the photomicrographs are shown in Figure 41. The area fraction method [62] was used to calculate an average V_f of 62%, which compares well with the literature data [2]. Table 12 lists the results obtained for each individual photo.

Photos #1 and #7 in Figure 41 reveal resin rich areas can be found throughout the cross-section. Further investigation of the local area in these photos revealed that the spacing between the resin rich areas was approximately equal to the thickness of the prepreg (125 μm). This agrees with Cattanach and Cogswell [26] who reported seeing resin rich layers in APC-2 where two prepregs have been joined by high process temperatures at short durations. Good fiber wetting was seen in all micrographs.

5.6 Matrix Microcracking

Transverse cracking was observed by x-ray radiography in the 7.6 mm x 50.8 mm strips cut from $[0_3/90_3]$ 25.4 mm x 152.4 mm APC-2 specimens, Figure 42. However, no cracks were observed in either of the as-processed (C1312A-2, C2312A-2, C3312N-1) or SFT cycled (SF1312D-2, SF2312D-1, SF3312D-2) full-scale specimens, Figures 43a and 43b.

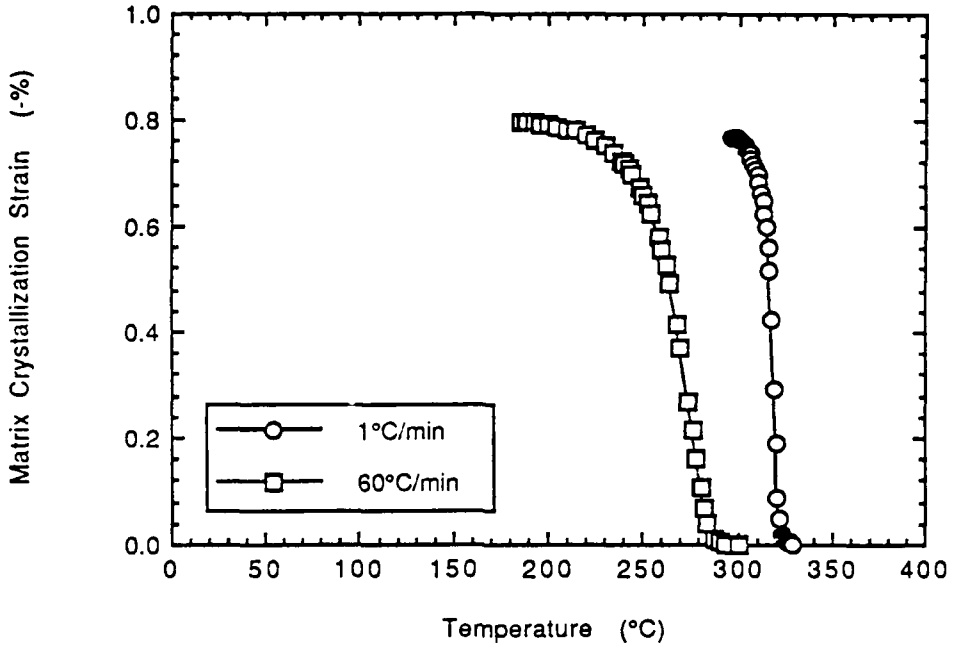

Figure 38. Matrix Crystallization Strain Development During Cool Down.

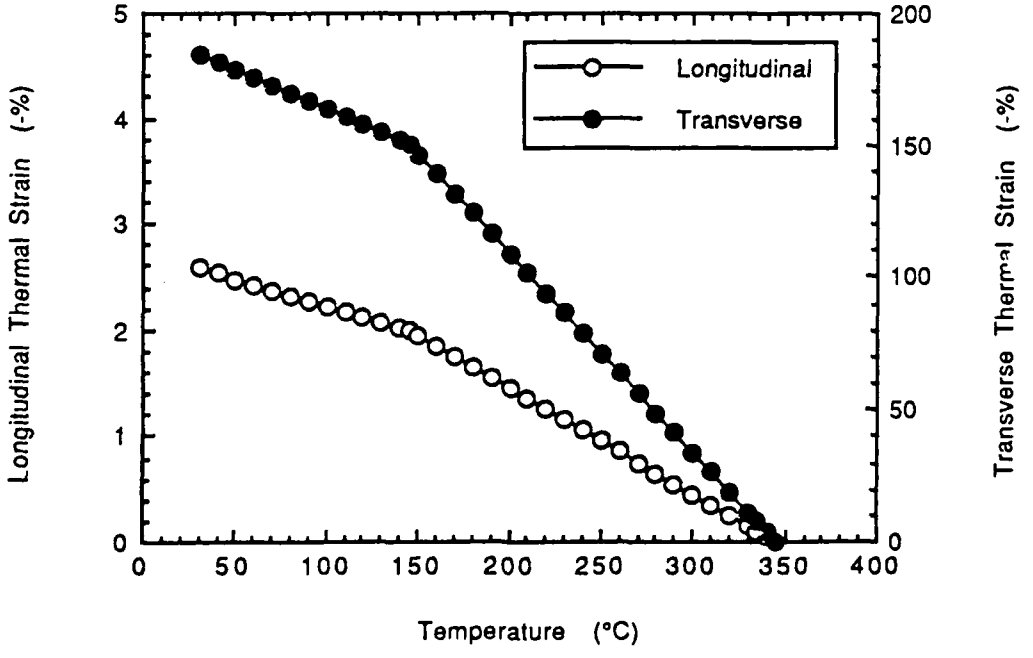

Figure 39. Longitudinal and Transverse Thermal Strain Development During Cool Down From the Melt Temperature.

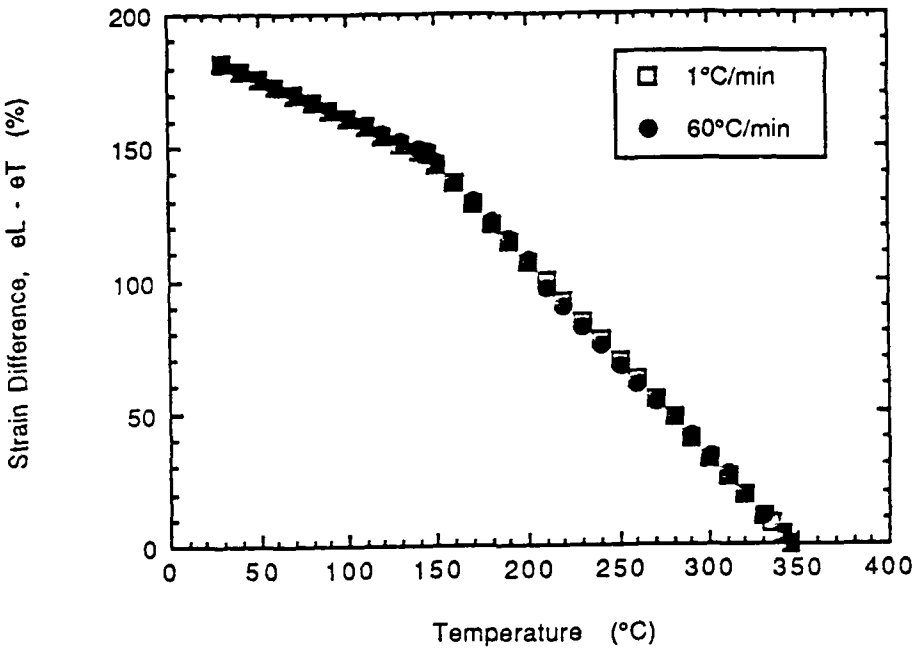

Figure 40. Strain Difference as a Function of Temperature and Process Cooling Rate.

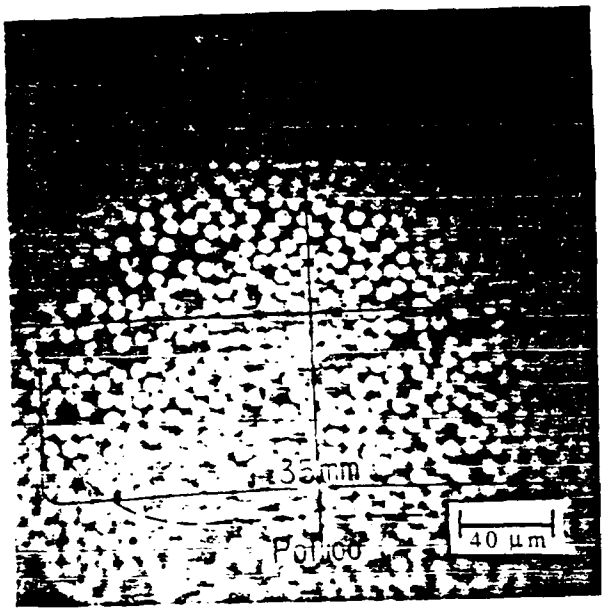

Photo #1 400X

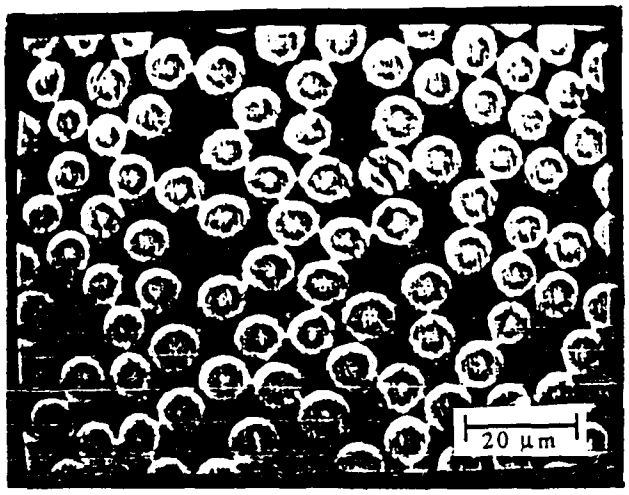

Photo #8 500X

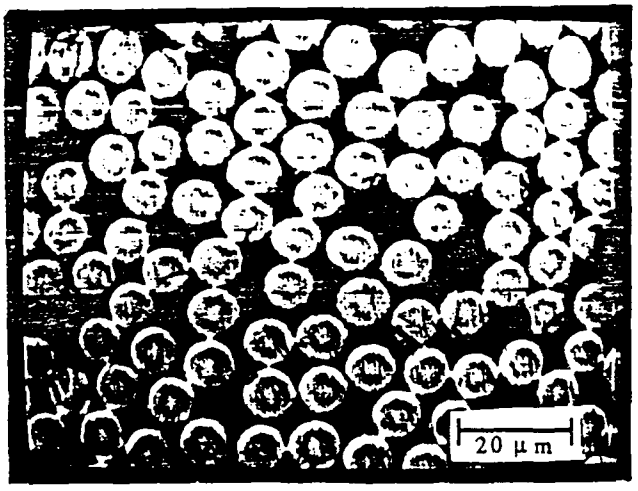

Photo #9 500X

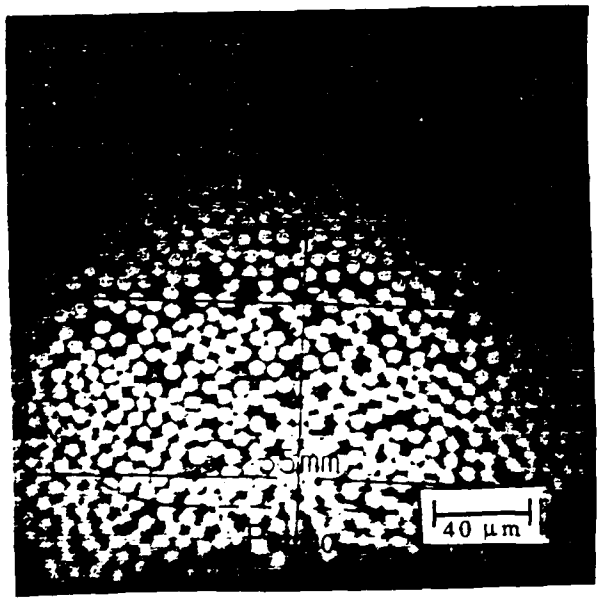

Photo #7 400X

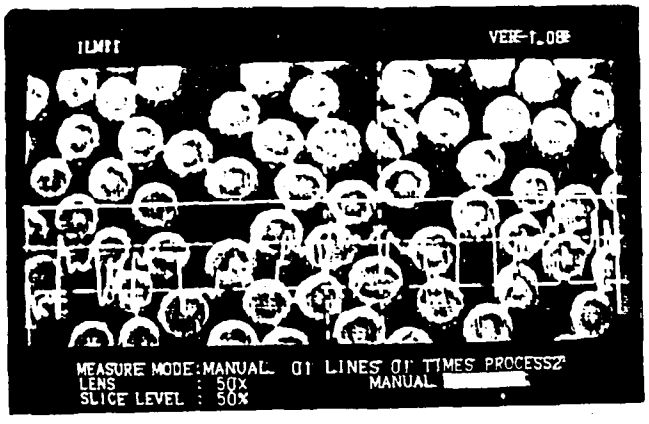

Photo #10 500X

Figure 41. Typical Photomicrographs from a Metallographic Microscope (left) and Scanning Laser Microscope (right) for a [0_6] APC-2 Specimen.

TABLE 12. APC-2 Fiber Volume Fraction.

LOCATION (Photo.Quadrant)	AREA of SELECTED REGION (μm)^2	NUMBER of FIBERS [D f = 7.2 μ m]	Vf FIBER VOLUME FRACTION (%)
1.1	5.96	130	57.27
1.3	5.96	151	66.53
1.4	5.96	146	64.32
2.4	5.96	129	56.83
3.4	5.96	151	66.53
4.3	5.96	122	53.75
5.4	5.96	139	61.24
6.1	5.96	136	59.92
6.3	5.96	139	61.24
7.1	5.96	128	56.39
7.3	5.96	139	61.24
7.4	5.96	138	60.80
8	3.28	83	66.53
9	3.28	90	72.14
10	2.08	53	66.84
		Average	62.10
		Standard Deviation	4.99
		Number of Samples	15

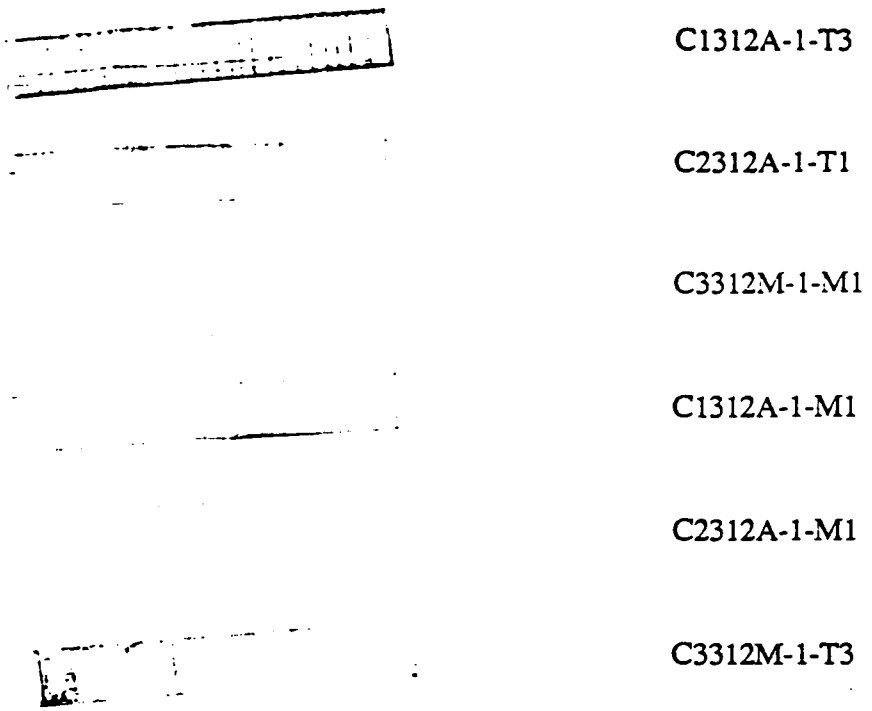

Figure 42. X-ray Radiograph of Cut-up [$0_3/90_3$] APC-2 Specimen.

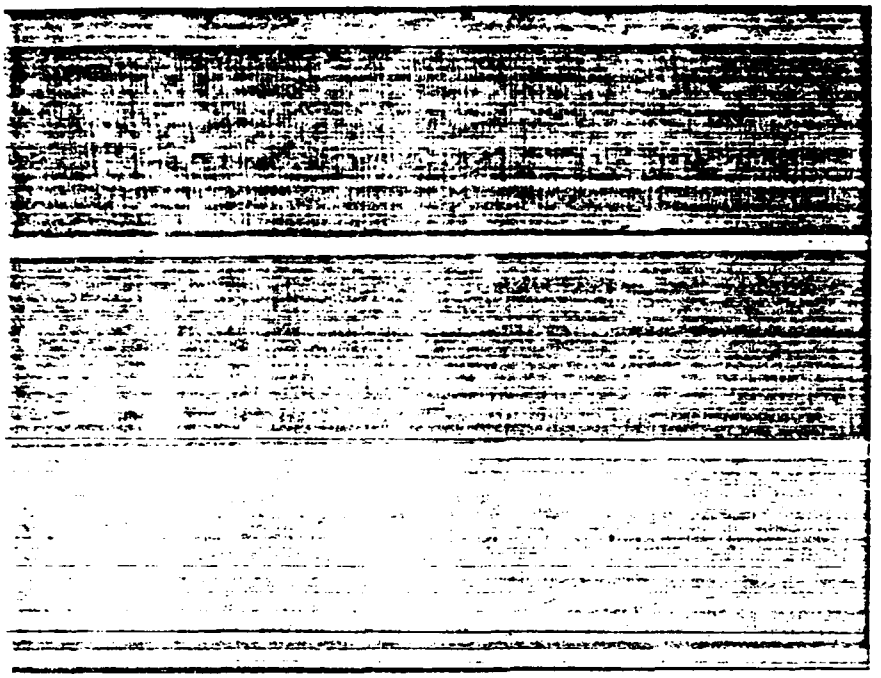

(a) As-Processed Full-Scale Specimens.

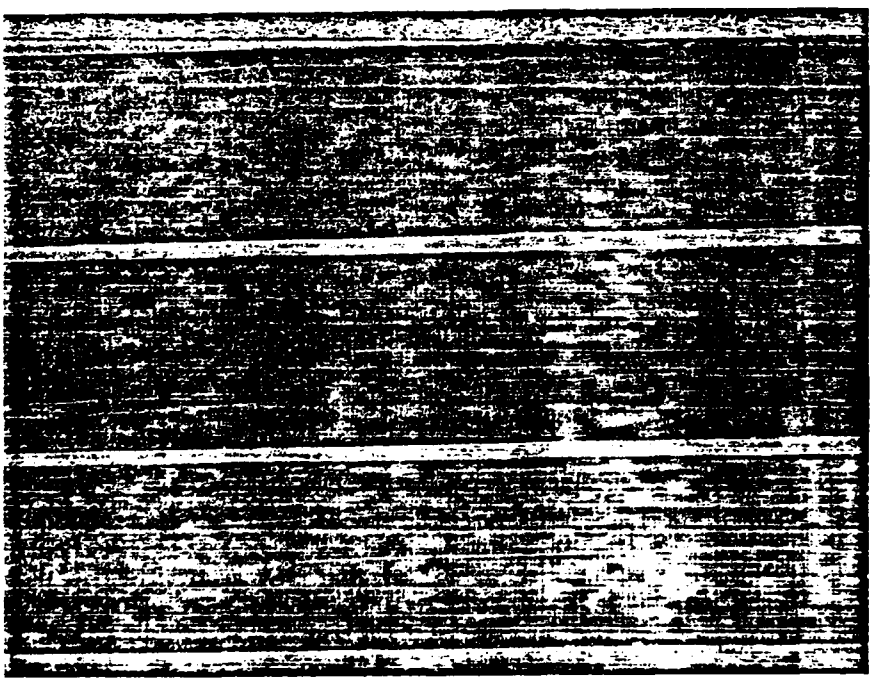

(b) Thermal Cycled Full-Scale Specimens.

Figure 43. X-ray Radiographs of Full-Scale [$0_3/90_3$] APC-2 Specimens.

This indicates that the thin strip specimens may have been traumatized during the cutting operation and the reporting of cracks in APC-2 by this method is misleading. The small hairline striations in the full-scale specimens are believed to be surface roughness effects and not transverse cracks. Transverse cracking due to residual stresses has been observed in other thermoplastic systems [55,60] while transverse cracking in APC-2 [56] was report as slight or none.

5.7 Elastic Analysis

The material properties given in Table 5 were used for all the elastic models discussed in Section 3.1. The temperature dependent transverse modulus of APC-2, Figure 44, was taken from Reference [56], where dynamic mechanical analysis at 3 Hz was used on a $[90_{24}]$ laminate. Values for $E_T(T)$ could not be monitored accurately above 280°C and should be taken as approximate. The results of modeling the dimensionless curvature by thermal-elastic analysis are shown in Figure 45 along with the experimental data from Figure 32.

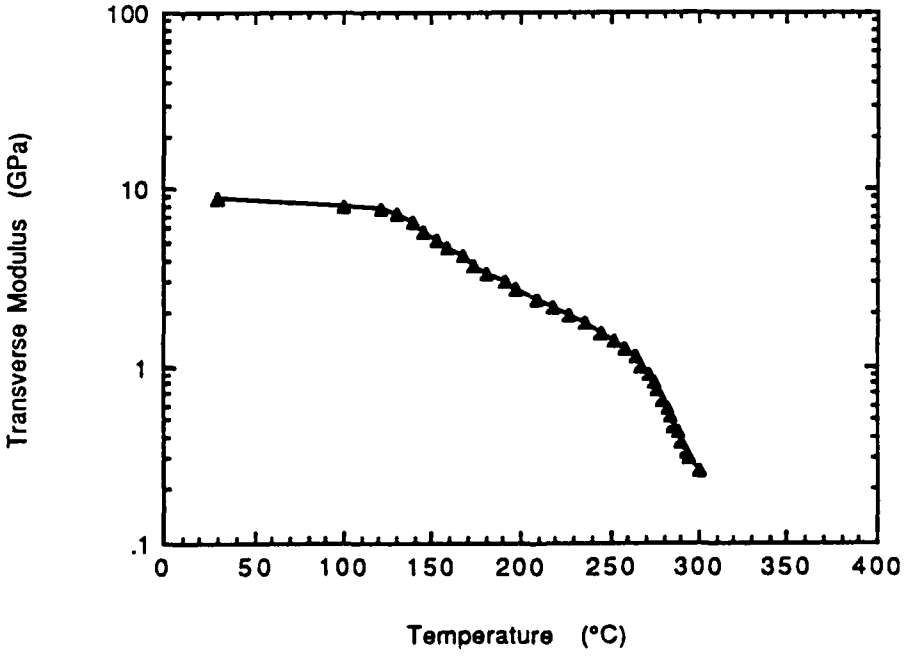

Figure 44. Dynamic Mechanical Measurement of the Temperature-Dependent Transverse Modulus E_T of APC-2 [56].

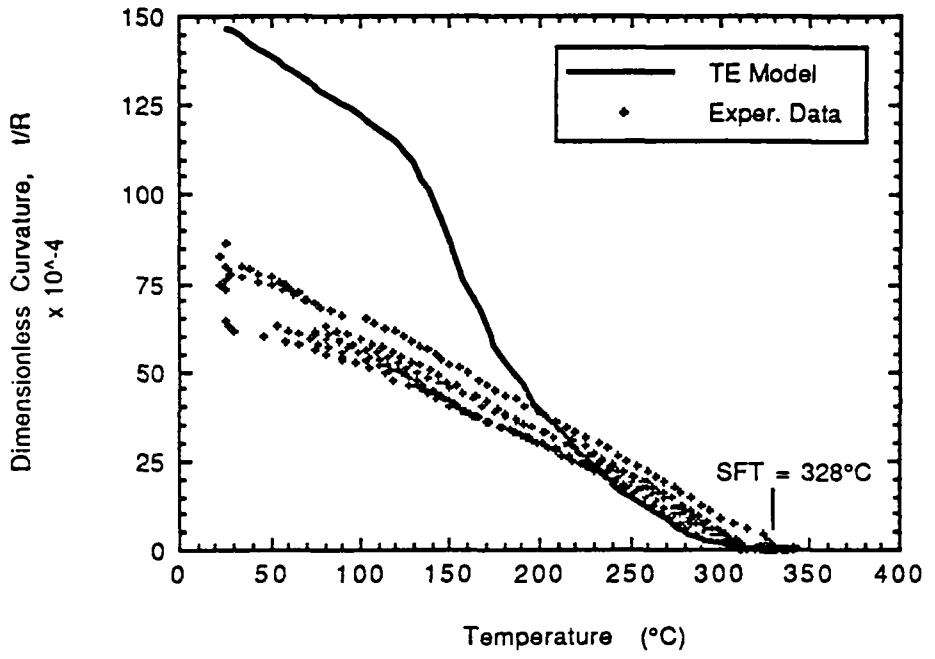

Figure 45. Dimensionless Curvature as Predicted by Laminated Plate Theory for Thin, Narrow Strips With Crystallization (Thermal-Elastic Model).

The modified laminate plate theory discussed in Section 3.1 incorporates thermal, geometric, and crystalline strain effects into a thermal-elastic model (TEM) using Eqs. (5), (6), (9), (10) and (15). The model over predicts the dimensionless curvature for temperatures lower than 190°C, but agrees well with the experimental data for temperatures between 200°C and T_m. The overestimate by the TEM at low temperatures is attributed to the large dependence on E_T in the geometry coefficient, on α_T in calculating the transverse thermal strains, and the neglect of stress relaxation effects. As seen previously, the transverse thermal strain dominates the development of residual stresses.

5.8 Viscoelastic Analysis

The input data for the viscoelastic (VE) model was obtained from tensile creep compliance data in the literature [31]. The tensile creep compliance master curve for 45G neat PEEK is reproduced in Figure 46 along with the shift factors associated with a reference temperature of 130°C. To the authors' knowledge, no creep data for APC-2 composites has been published in the open literature. Because the neat PEEK master curve has a distinct knee at approximately 5×10^6 seconds, the curve was analyzed as two linear regions. Figures 47 and 48 show the linear regression performed on the master curve below and above the knee. These regression parameters were input into the VE model as well as the transverse compliance at t_o and t_{knee}. The input properties for the model are listed in Table 13.

Table 14 lists the room temperature curvature predictions for cooling at rates of 0.54, 60, and 700°C/min. The final curvatures differ by only 5% and are seen to increase with increasing cooling rates. The VE model prediction of t/R for cooling at 1°C/min is shown in Figure 49 along with the experimental data obtained in the SFT study. While the viscoelastic analysis does provide a more precise description of the PEEK matrix, it is seen to under predict the residual stresses during the onset of crystallization and overestimate the stresses at temperatures below T_{ec}, similar to the results found using the TE model.

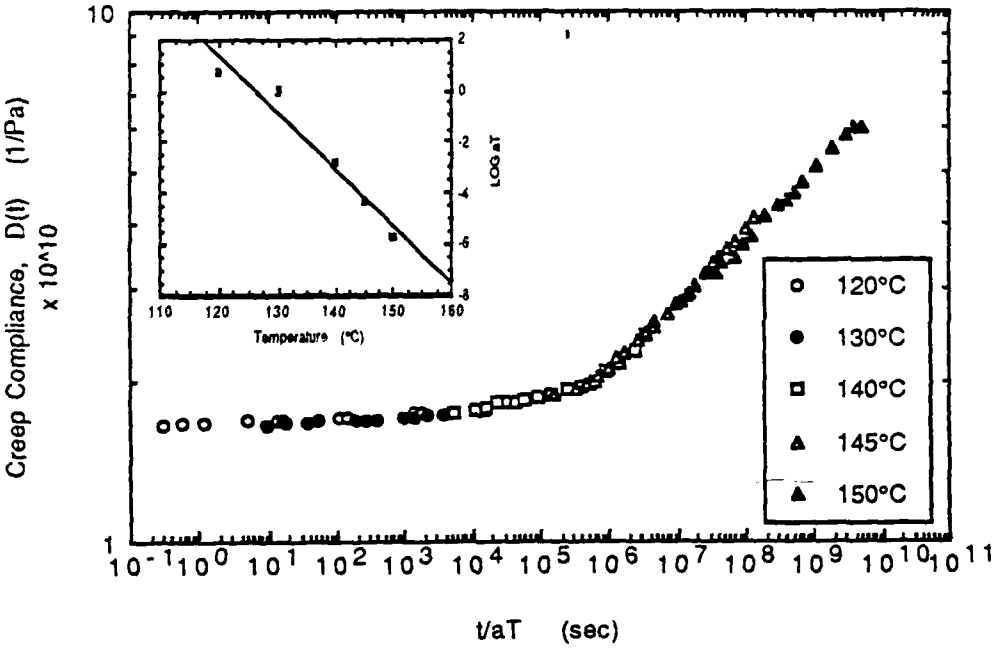

Figure 46. Tensile Creep Compliance Master Curve for 33% Crystalline Neat PEEK for Testing Times of 10^4 sec (T_{ref}=130°C) [31].

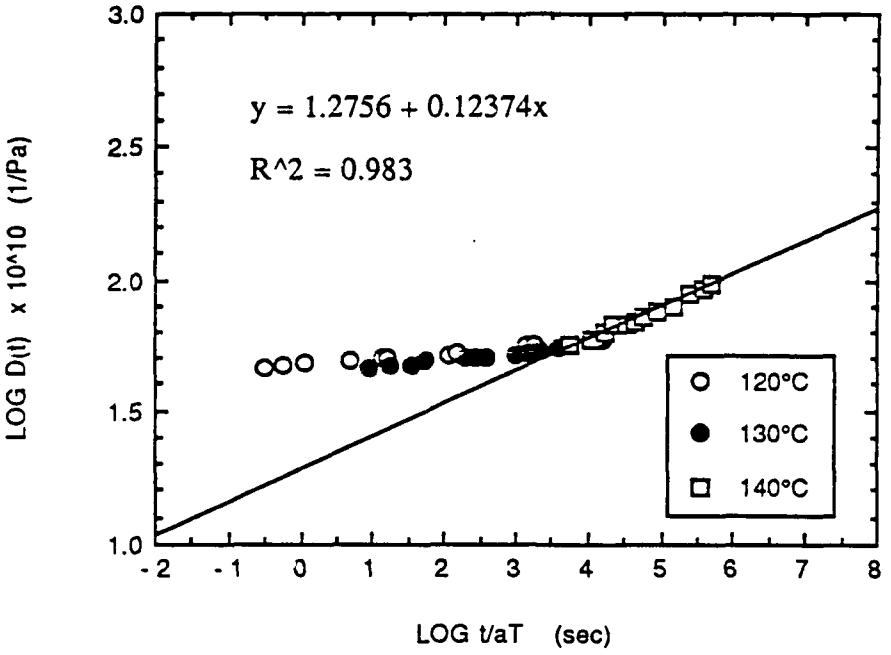

Figure 47. Tensile Creep Compliance for t/a_T Below the Master Curve Knee.

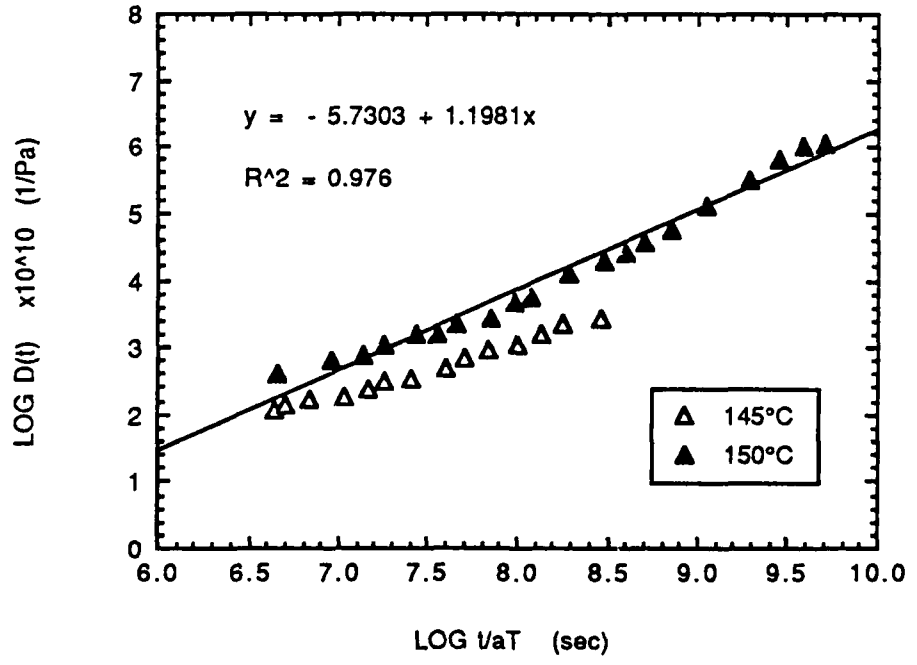

Figure 48. Tensile Creep Compliance for t/a_T Above the Master Curve Knee.

Table 13. Viscoelastic Model Input Properties.

Shift Factor Parameters:	A = 4.486 B = 89.035
Stress-Free Temperature, T_{sf}	328°C
Room Temperature, T_{rm}	28°C
Longitudinal Compliance, S_{11}	7.396 (10^{-12}) Pa^{-1}
Shear Compliance, S_{12}	2.589 (10^{-12}) Pa^{-1}
Transverse Compliance Intercept, D°	1.087 (10^{-10}) Pa^{-1}
Transverse Compliance at Knee, D*	1.980 (10^{-10}) Pa^{-1}
$\log\left(t/a_T\right)_{knee}$	5.681 sec
Transverse Compliance Curve Fit Parameters (below knee)	D_L = 1.778 (10^{-9}) (Pa sec^n)$^{-1}$ n_L = 0.1237
Transverse Compliance Curve Fit Parameters (above knee)	D_U = 0.119 (10^{-10}) (Pa sec^n)$^{-1}$ n_U = 1.1981

Table 14. Viscoelastic Predictions of Dimensionless Curvature at Room Temperature for APC-2 Laminates.

Q_c Cooling Rate (°C/min)	Δt Time Increment (sec)	t/R Dimensionless Curvature (x 10-4)
0.54	111	98.22
60.00	1	98.20
700.00	8.571(10^{-2})	98.02

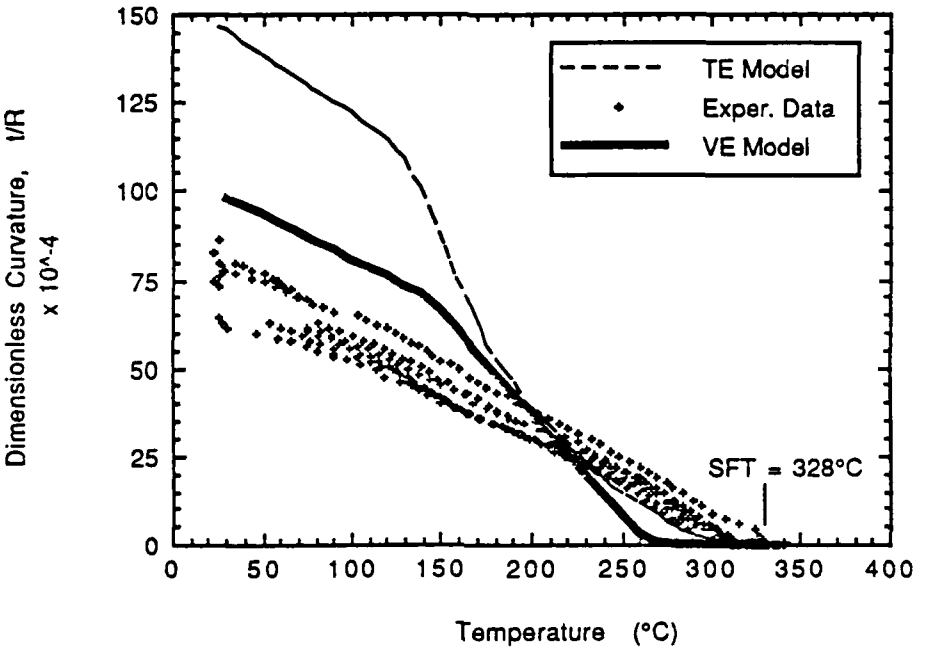

Figure 49. Prediction of Dimensionless Curvatures by Viscoelastic Model (VE Model) as a Function of Cool Down Temperature.

6. CONCLUSIONS

The dimensionless curvature has been used as an indicator of residual stress in asymmetric cross-ply laminates. The process cooling rate was found to influence the amount of residual stresses present in AS4/PEEK composites. Higher cooling rates result in lower crystallinity and, hence, lower crystallization shrinkage. The transverse thermal strain was seen to dominate over both the transverse crystallization strain and the stress relaxation effects.

The recommended process temperature and dwell time were 380°C and 30 minutes, respectively. The dwell time may be shortened to 10-15 minutes for thin laminates ($t < 0.15$ cm). It is not known what relationship exists between the dwell time and laminate thickness is $t > 5$ cm. The pressure applied during as-processed conditions appears to have no influence on the amount of residual stresses. A constant pressure of 200 psi provided consistent high quality specimens.

The stress-free temperature of as-processed $[0_3/90_3]$ APC-2 laminates decreased with increasing process cooling rate. The SFT for any heating cycle was found to be equivalent to the previous cooling cycle SFT. Constrained heating/cooling (e.g. annealing) resulted in the stress relaxation of specimens with high as-processed residual stresses. Thus, when pressure is applied the specimen is under additional mechanical strains to remain flat reducing the amount of thermal and crystallization shrinkage developed; therefore, stress relaxation effects dominate and the curvature is decreased. Hence, the SFT is strongly dependent on the previous temperature and pressure histories and the proper selection of the SFT is necessary for accurate model predictions.

The thermal-elastic model used laminated plate theory with modifications accounting for temperature, geometry, and crystallinity effects. The model agrees well with the experimental data for temperatures greater than 180°C, but grossly overestimates the dimensionless curvature below T_g since it does not consider stress relaxation effects.

The viscoelastic model used in this study [66] is for linear viscoelastic behavior. The model over predicts the amount of stress relaxation occurring at high temperatures near the onset of crystallization and thus, underestimates the specimen curvature. Likewise, the model overestimates the stresses at temperatures below T_g. There is inconclusive evidence at this time that the presence of transverse cracking may account for the overestimate and, hence, additional work must done in this area. A room-temperature dimensionless curvature of 98×10^{-4} is predicted for $[0_3/90_3]$ 25 mm x 152 mm APC-2 laminates having a SFT of 328°C and cooled at a rate of 1°C/min.

7. RECOMMENDATIONS FOR FUTURE WORK

The effects of annealing under loading need to be investigated in order to provide an optimum process cycle for the reduction of residual stresses and increased structural integrity of AS4/PEEK composites. The presence of transverse cracking in APC-2 laminates should be investigated with respect to processing variables (e.g. cooling rate and annealing). In addition, the creep behavior of APC-2 needs to be obtained as opposed to the use of neat PEEK properties. The results would then be incorporated into the viscoelastic model to provide a more complete understanding of the development of process-induced residual stresses in thermoplastic composites.

Fiber microbuckling is frequently observed even in compression molding of flat laminates. The formation, prevention, and effects on structural integrity of fiber microbuckling should be investigated for thermoplastic matrix composites. Specifically, graphite/PEEK systems are of importance because of their increased structural use in the aircraft and aerospace industries.

8. REFERENCES

1. G. R. Belbin, I. Brewster, F. N. Cogswell, D. J. Hezzell, and M. S. Swerdlow, "Carbon Fiber Reinforced Polyether Etherketone: A Thermoplastic for Aerospace Applications," *SAMPE Conference*, Stresa, Italy, 1982.
2. A. Cervenka, "PEEK/Carbon Fiber Composites: Experimental Evaluation of Unidirectional Laminates and Theoretical Prediction of Their Properties," *Polymer Composites*, Vol. 9, No. 4, August 1988, pp. 263-270.
3. S. W. Tsai, *Composites Design*, 4th Ed., Think Composites, Dayton, OH, 1988.
4. G. C. McGrath, D. W. Clegg and A. A. Collyer, "The Mechanical Properties of Compression Moulded Reconstituted Carbon Fibre Reinforced PEEK (APC-2)," *Composites*, Vol. 19, No. 3, May 1988, pp. 211-216.
5. S. P. Grossman and M. F. Amateau, "The Effect of Processing on a Graphite Fiber/Polyetheretherketone Thermoplastic Composite," *33rd International SAMPE Symposium*, 7-10 March 1988, pp. 681-692.
6. D. Purslow, "Matrix Fractography of Fibre-reinforced Thermoplastics, Part 1. Peel Failures," *Composites*, Vol. 18, No. 5, November 1987, pp. 365-374.
7. R. J. Lee, "Compression Strength of Carbon Fibre-reinforced Thermoplastic Laminates," *Composites*, Vol. 18, No. 1, January 1987, pp. 35-39.
8. D. C. Leach, D. C. Curtis and D. R. Tamblin, "Delamination Behavior of Carbon Fiber/Poly(etheretherketone) (PEEK) Composites," *Toughened Composites, ASTM 937*, N. J. Johnston, Ed., American Society for Testing and Materials, Philadelphia, PA, 1987, pp. 358-380.
9. D. F. Adams and D. A. Crane, "Combined Loading Micromechanical Analysis of a Unidirectional Composite," *Composites*, Vol. 15, No. 3, July 1984, pp. 181-192.
10. J. A. Nixon, M. G. Phillips, D. R. Moore and R. S. Prediger, "A Study of the Development of Impact Damage in Cross-ply Carbon Fibre/PEEK Laminates Using Acoustic Emission," *Composites Science and Technology*, Vol. 31, 1988, pp. 1-14.
11. C. K. L. Davies, S. Turner and K. H. Williamson, "Flexed Plate Impact Testing of Carbon Fibre-Reinforced Polymer Composites," *Composites*, Vol. 16, No. 4, October 1985, pp. 279-285.
12. P. E. Reed and S. Turner, "Flexed Plate Impact, Part 7. Low Energy and Excess Energy Impacts on Carbon Fibre-Reinforced Polymer Composites," *Composites*, Vol. 19, No. 3, May 1988, pp. 193-203.

13. J. W. Gillespie Jr., L.A. Carlsson and A. J. Smiley, "Rate-Dependent Mode I Interlaminar Crack Growth Mechanisms in Graphite/Epoxy and Graphite/PEEK," *Composites Science and Technology*, Vol. 28, 1987, pp. 1-15.
14. A. J. Smiley and R. B. Pipes, "Rate Sensitivity of Mode II Interlaminar Fracture Toughness in Graphite/Epoxy and Graphite/PEEK Composite Materials," *Composites Science and Technology*, Vol. 29, 1987, pp. 1-15.
15. S. L. Donaldson, "Fracture Toughness Testing of Graphite/Epoxy and Graphite/PEEK Composites," *Composites*, Vol. 16, No. 2, April 1985, pp. 103-112.
16. D. C. Curtis, D. R. Moore, B. Slater and N. Zahlan, "Fatigue Testing of Multi-angle Laminates of CF/PEEK," *Composites*, Vol. 19, No. 6, November 1988, pp. 446-452.
17. T. K. O'Brien, "Fatigue Delamination Behavior of PEEK Thermoplastic Composite Laminates," *J. of Reinforced Plastics and Composites*, Vol. 7, No. 4, July 1988, pp. 341-359.
18. D. Purslow, "Matrix Fractography of Fibre-reinforced Thermoplastics, Part 2. Shear Failures," *Composites*, Vol. 19, No. 2, March 1988, pp. 115-126.
19. D. Purslow, "Matrix Fractography of Fibre-reinforced Thermoplastics, Part 3. Tensile, Compressive and Flexural Failures," *Composites*, Vol. 19, No. 5, September 1988, pp. 358-366.
20. J. C. Seferis and C. N. Velisaris, "Modeling-Processing-Structure Relationships of Polyetheretherketone (PEEK) Based Composites," *31st International SAMPE Symposium*, 7-10 April 1986, pp. 1236-1252.
21. W. H. M. van Dreumel and M. de Groot, "An Experimental Nose-wheel Door of Continuous Fibre-Reinforced Thermoplastic," *Composites*, Vol. 18, No. 5, November 1987, pp. 405-408.
22. Hercules Product Data Sheet, No. 847-4, Hercules, Inc.
23. D. J. Blundell, J. M. Chalmers, M. W. Mackenzie and W. F. Gaskin, " Crystalline Morphology of the Matrix of PEEK-Carbon Fiber Aromatic Polymer Composites I. Assessment of Crystallinity," *SAMPE Quarterly*, Vol. 16, No. 4, July 1985, pp. 22-30.
24. D. J. Blundell and B. N. Osborn, "Crystalline Morphology of the Matrix of PEEK-Carbon Fiber Aromatic Polymer Composites II. Crystallization Behavior," *SAMPE Quarterly*, Vol. 17, No. 1, October 1985, pp. 1-6.
25. J. A. Nairn and P. Zoller, "Residual Thermal Stresses in Semicrystalline Thermoplastic Matrix Composites," *Proceedings of Fifth International Conference on Composite Materials*, San Diego, CA, August 1985, pp. 931-946.

26. J. B. Cattanach and F. N. Cogswell, "Processing with Polymer Composites," *Developments in Reinforced Plastics*, G. Pritchard ed., Vol. 5, Elsevier Publishing, London, 1986, pp.1-38.
27. P. Zoller, "Solidification Processes in Thermoplastics and Their Role in the Development of Internal Stresses in Composites," *Proceedings of the American Society for Composites, Third Technical Conference*, Technomic Publishing, Lancaster, PA, 1989, pp. 439-448.
28. E. J. Staber, J.C. Seferis, and J. D. Keenam, "Characterization and Exposure of Polyetheretherketone (PEEK) to Fluid Environments," *Polymer*, Vol. 25, 1984, p. 1845.
29. J. T. Hartness, "Polyetheretherketone Matrix Composites," *SAMPE Quarterly*, Vol. 14, No. 2, January 1983, pp. 33-37.
30. W. Sichina, "Time-Temperature Superpositioning Studies of Thermoplastic Composites," *SPE ANTEC '88 Conference Proceedings*, Atlanta, GA, April 1988, pp.1139-1142.
31. A. A. Ogale and R. L. McCullough, "Influence of Microstructure on Elastic and Viscoelastic Properties of Polyether Ether Ketone," *Composites Science and Technology*, Vol. 30, June 1987, pp. 185-201.
32. Z. Hashin, E. A. Humphreys and J. Goeing, "Analysis of Thermoviscoelastic Behavior of Unidirectional Fiber Composites," *Composites Science and Technology*, Vol. 29, 1987, pp. 103-131.
33. B. D. Harper and Y. Weitsman, "Residual Thermal Stresses in an Unsymmetric Cross-ply Graphite/Epoxy Laminates," *Proceedings AIAA/ASME/ASCE/AHS 22nd SSDM Conference*, 1981, p. 325.
34. D. L. Flaggs and F. W. Crossman, "Analysis of the Viscoelastic Response of Composite Laminates During Hygrothermal Exposure," *J. of Composite Materials*, Vol. 15, 1981, p. 286.
35. Y. Weitsman, "Optimal Cool-Down in Linear Viscoelasticity," *J. Applied Mechanics*, Vol. 47, 1980, p. 35.
36. T. J. Chapman, J. W. Gillespie, Jr., R. B. Pipes, J-A. E. Manson and J. C. Seferis, "Thermal Skin/Core Residual Stresses Induced During Cooling of Thermoplastic Matrix Composites," *Proceedings of the American Society for Composites, 3rd Technical Conference*, Technomic Publishing, Lancaster, PA, 1988, pp.449-458.
37. J. C. Seferis, "Polyetheretherketone (PEEK): Processing-Structure and Properties Studies for a Matrix in High Performance Composites," *Polymer Composites*, Vol. 7, No. 3, June 1986, pp. 158-169.
38. P. Cebe, S.-D. Hong, S. Chung and A. Gupta, "Mechanical Properties and Morphology of Poly(etheretherketone)," *Toughened Composites, ASTM 937*, N. J. Johnston, Ed., American Society for Testing and Materials, Philadelphia, PA, 1987, pp. 342-357.

39. W. I. Lee, M. F. Talbott, G. S. Springer and L. A. Berglund, "Effects of Cooling Rate on the Crystallinity and Mechanical Properties of Thermoplastic Composites," *Advances in Modeling of Composite Processes*, Technomic Publishing, Lancaster, PA, 1986, pp. 119-128.
40. S. M. Grove, "Thermal Modeling of Tape Laying with Continuous Carbon Fibre-Reinforced Thermoplastic," *Composites*, Vol. 19, No. 5, September 1988, pp. 367-375.
41. J. C. Seferis, C. Ahlstrom, and S. H. Dillman, "Cooling Rate and Annealing as Processing Parameters for Semicrystalline Thermoplastic-Based Composites," *SPE ANTEC '87 Conference Proceedings*, Los Angeles, CA, May 1987, pp. 1467-1471.
42. R. J. Downs and L. A. Berglund, "Apparatus for Preparing Thermoplastic Composites," *J. of Reinforced Plastics and Composites*, Vol. 6, January 1987, pp.89-99.
43. J. C. Seferis and C. N. Velisaris, "Thermal Processing and Characterization of Polyetheretherketone (PEEK) Matrices," *SPE ANTEC '85 Conference Proceedings*, 1985, pp.401-403.
44. J. A. Nairn, "Thermoelastic Analysis of Residual Stresses in Unidirectional, High-Performance Composites," *Polymer Composites*, Vol. 6, No. 2, April 1985, pp.123-130.
45. J. C. Seferis and C. N. Velisaris, "Crystallization Kinetics of Polyetheretherketone (PEEK) Matrices," *Polymer Engineering and Science*, Vol. 26, No. 22, December 1986, pp. 1574-1581.
46. D. J. Blundell and F. M. Willmouth, "Crystalline Morphology of the Matrix of PEEK-Carbon Fiber Aromatic Polymer Composites," *SAMPE Quarterly*, Vol. 17, No. 2, January 1986, pp. 50-57.
47. P. Cebe and S.-D. Hong, "Crystallization Behavior of Poly(etheretherketone)," *Polymer*, Vol. 27, August 1986, pp. 1183-1192.
48. D. J. Blundell and B. N. Osborn, "The Morphology of Poly(aryl-ether-ether-ketone)," *Polymer*, Vol. 24, August 1983, pp. 953-958.
49. N. G. McCrum, C. P. Buckley and C. B. Bucknall, *Principles of Polymer Engineering*, Oxford University Press, New York, 1988.
50. P. Cebe, "Non-Isothermal Crystallization of Poly(Etheretherketone) Aromatic Polymer Composite," *Polymer Composites*, Vol. 9, No. 4, August 1988, pp. 271-279.
51. F. N. Cogswell, "Microstructure and Properties of Thermoplastic Aromatic Polymer Composites," *SAMPE Quarterly*, July 1983, pp. 33-37.
52. H. T. Hahn, S. R. White, and K. J. Schulte, "Prediction and Control of Processing-Induced Residual Stresses," *Composites Manufacturing Technology Center, Report CMTC-88-25*, The Pennsylvania State University, 31 December 1988.

53. M. W. Hyer, "The Room-Temperature Shapes of Four-Layer Unsymmetric Cross-Ply Laminates," *J. of Composite Materials*, Vol.16, 1982, p. 318.
54. H. T. Hahn, "Warping of Unsymmetric Cross-Ply Graphite/Epoxy Laminates," *Composites Technology Review*, Vol. 3, 1981, p. 114.
55. J. A. Nairn and P. Zoller, "The Development of Residual Thermal Stresses in Amorphous and Semicrystalline Thermoplastic Matrix Composites," *Toughened Composites, ASTM STP 937*, N. J. Johnston, Ed., American Society for Testing and Materials, Philadelphia, PA, 1987, pp. 328-341.
56. G. Jeronimidis and A. T. Parkyn, "Residual Stresses in Carbon Fibre-Thermoplastic Matrix Laminates," *J. of Composite Materials*, Vol. 22, No. 5, May 1988, pp. 401-415.
57. I. M. Daniel J. L. Mullineaux, F. J. Ahimaz, and T. Liber, "The Embedded Strain Gage Technique for Testing Boron/Epoxy Composites," *Composite Materials: Testing and Design, Second Conference, ASTM STP 497*, 1972, pp. 257-272.
58. R. Y. Kim and H. T. Hahn, "Effect of Curing Stresses on the First Ply-Failure in Composite Laminates," *J. of Composite Materials*, Vol. 13, No. 2, 1979.
59. J-A. E. Manson and J. C. Seferis, "Internal Stress Determination by Process Simulated Laminates," *SPE ANTEC '87 Conference Proceedings*, Los Angeles, CA, May 1987, pp. 1446-1449.
60. K. S. Kim and H. T. Hahn, "The Effect of Cooling Rate on Residual Stresses in Thermoplastic Composites," *J. of Composite Technology and Research*, Vol. 11, No. 2, Summer 1989, pp. 47-52.
61. *CRC Standard Mathematical Tables*, 28th Edition, CRC Press, Inc., 1987.
62. L.A. Carlsson and R. B. Pipes, *Experimental Characterization of Advanced Composite Materials*, Prentice-Hall, Inc., 1987, pp. 45-52.
63. H. T. Hahn and N. J. Pagano, "Curing Stresses in Composite Laminates," *J. of Composite Materials*, Vol. 9, 1975, p. 91.
64. N. J. Pagano and H. T. Hahn, "Evaluation of Composite Curing Stress," *Composite Materials: Testing and Design , Fourth Conference, ASTM STP 617*, 1977, p. 317.
65. S. Timoshenko, "Analysis of Bi-Metal Thermostats," *J. of the American Optical Society*, Vol. 11, September 1925, pp. 233-255.
66. S. R. White and H. T. Hahn, "Prediction and Control of Processing-Induced Residual Stresses in Composites, Part I. IM6/BMI Composite," *Composites Manufacturing Technology Center, Report CMTC-89-45*, The Pennsylvania State University, September 1989.

67. P. J. Mallon and C. M. O'Bradaigh, "Development of a Pilot Autoclave for Polymeric Diaphragm Forming of Continuous Fibre-Reinforced Thermoplastics," *Composites*, Vol. 19, No. 1, January 1988, pp. 37-47.
68. P. J. Mallon, C. M. O'Bradaigh and R. B. Pipes, "Polymeric Diaphragm Forming of Complex-Curvature Thermoplastic Composite Parts," *Composites*, Vol. 20, No. 1, January 1989, pp. 48-56.
69. H. T. Hahn, S. R. White, and K. J. Schulte, "Process Optimization for Improved Structural Integrity," Technical Proposal, submitted to Air Force Office of Scientific Research, 1 June 1989.
70. W. C. Dale and E. Baer, "Fiber Buckling in Composite Systems: A model for the Ultrastructure of Unsalified Collagen Tissues," *J. of Material Science*, Vol. 9, No. 3, 1974, p. 369.
71. W. I Lee and G. S. Springer, " A Model of the Manufacturing Process of Thermoplastic Matrix Composites," *J. of Composite Materials*, Vol. 18, No. 4, 1984, p. 1055.
72. M. F. Talbott, G. S. Springer, and L. A. Berglund, "The Effects of Crystallinity on the Mechanical Properties of PEEK Polymer and Graphite Fiber Reinforced PEEK," *J. of Composite Materials*, Vol. 21, November 1987, pp.1056-1081.
73. S. W. Tsai and H. T. Hahn, *Introduction to Composite Materials*, Technomic Publishing Company, Inc., 1980.